Abstract

The performance of integrated optical waveguide sensor devices is strongly dependent on efficient coupling of light into and out of the waveguide. To avoid the time-consuming alignment procedures of lenses or prisms, it is beneficial to find new coupling methods. Within the frame of this work an approach using fluorescent molecules as secondary emitters inside the waveguide and scattering material to deflect the light to a detecting device was investigated. A light emitting diode excites the fluorescent molecules, which couple light into the waveguide. The out-coupled light is detected by an integrating sphere coupled to a spectrometer.

A chapter on the theoretical foundations gives a basic overview on waveguide physics, discussing both the geometrical and the electromagnetical approach, leading to the concept of optical modes and providing an overview of coupling methods. Furthermore, the profile and number of transverse electric modes was analyzed numerically by solving the transcendental equation for an asymmetrical infinite slab waveguide. Raytracing simulations of the propagation of light originating from an isotropic point source conclude the theoretical part.

A planar waveguide structure consisting of a polystyrene core and a polydimethylsiloxane cladding fabricated by spin coating and knife coating was used to investigate the influence of different parameters on the throughput, which is the combined effect of light in- and out-coupling. In order to couple light efficiently into the waveguide a two component fluorophore resonance energy transfer system was optimized by varying the molecule concentration inside a matrix material. Two different drop coating techniques were compared to apply the molecules to the core material revealing that the molecules should be included into the waveguide. Furthermore, by varying the spin coating rotation speed, the influence of the thickness of the core material was investigated. It was observed that a thicker waveguide yields a higher throughput of light. The intensity of the excitation source does not affect the throughput. In addition to end-face coupling, an alternative out-coupling method utilizing scattering material was investigated. Titanium oxide was deposited on top of the core material and the attenuated light intensity emitted from the edge of the waveguide was measured. It turns out that even a scattering width of a few millimeters attenuates the signal to a few percent. As a proof of principle it was shown that light is coupled out by the scatterer and can be measured directly.

Abstract

Die Effizienz eines integrierten optischen Wellenleitersensorsystems ist abhängig von effektiver Ein- und Auskopplung von Licht in den Wellenleiter. Da die Verwendung von Linsen und Prismen aufgrund der notwendigen Justierung zeitaufwendig ist und nicht zur Kompaktheit des Systems beiträgt, ist es wichtig nach alternativen Methoden zu suchen. Fluoreszierende Moleküle, die sich in der Wellenleiterschicht befinden, und Streupartikel zur Umlenkung des Lichts zu einem Detektor, bieten einen alternativen Ansatz. Mittels einer Leuchtdiode werden die Sekundäremitter angeregt, um Licht in den Wellenleiter zu koppeln. Am anderen Ende des Wellenleiters wird das ausgekoppelte Licht mit einem an eine Ulbrichtkugel angeschlossenen Spektrometer detektiert.

Ein theoretisches Kapitel bietet Grundlagen zur Wellenleiterphysik in Form eines Vergleichs von geometrischer mit elektromagnetischer Optik. Neben einer Betrachtung der grundlegenden Eigenschaften von optischen Moden wird ein Überblick über verschiedene Kopplungsmethoden geboten. Das Profil von transversal elektrischen Moden wird durch Lösung der transzendenten Gleichung für einen planaren Wellenleiter numerisch ausgewertet. *Ray tracing* Simulationen zur Ausbreitung von Licht einer isotropen Punktlichtquelle leiten zum experimentellen Teil über.

Ein planares Wellenleitersystem, bestehend aus einem Polystyrol Wellenleiter und einem Polydimethylsiloxan Cladding, wurde verwendet, um den Einfluss verschiedener Parameter auf den Lichtdurchsatz zu bestimmen. Die Herstellung des Schichtsystems erfolgte mittels spin coating und einer Spiralrakeltechnik. Um Licht effizient in den Wellenleiter einzukoppeln, wurde eine Optimierung des Resonanzenergietransfers zweier Fluorophore durchgeführt. Die Analyse von zwei verschiedenen Auftropftechniken führte zum Ergebnis, dass fluoreszierende Moleküle in den Wellenleiter inkludiert sein sollten. Durch eine Variation der spin coating Geschwindigkeit wurde der Einfluss der Schichtdicke des Wellenleiters auf den Lichtdurchsatz untersucht. Ein dicker Wellenleiter führt zu einem größeren Lichtdurchsatz, die Intensität der Anregung beeinflusst den Lichtdurchsatz hingegen nicht. Als Alternative zur Auskopplung des Lichts an der Kante des Wellenleiters wurden Streupartikel verwendet. Titanoxidschichten variierender Breite wurden auf die Oberseite des Wellenleiters aufgebracht und anschließend die Intensitätsabschwächung des Lichts an der Kante gemessen. Streifen von einigen Millimetern Breite genügen bereits, um das Signal an der Kante auf wenige Prozent zu dämpfen. Im Anschluss daran wurde gezeigt, dass das von den Titanoxidschichten gestreute Licht direkt gemessen werden kann.

Acknowledgement

First of all, I want to thank my supervising tutor Ao.Univ.-Prof. Dr. Joachim Krenn for all the guidance and assistance throughout my work at Joanneum Research. I want to acknowledge him and DI Dr. Georg Jakopic for allowing me to attend the SPIE Photonics Europe conference. Furthermore, I want to thank Mag. Dr. Bernhard Lamprecht for introducing me to the subject and the equipment and helping me during my ten months in Weiz, DI Dr. Volker Schmidt for assisting me with the optical simulation software ZEMAX and Dr. Torsten Mayr and DI Tobias Abel for offering the basic ideas for this work. Last but not least, thanks to my parents for their help and support during my studies.

Contents

Chapter 1

Introduction

In integrated optical waveguide sensor devices efficient coupling of light into and out of a waveguide structure is an important issue. As for waveguides with thicknesses in the order of a few micrometers the arrangement of prisms or lenses is a complicated and time consuming task, new ways for coupling light into waveguides have to be found. Fluorescent dyes and scattering molecules provide the deflection which is needed when the excitation source and the detector are integrated in the sensor. The fluorescence resonance engery transfer inside a two component system (Macrolex Yellow and Macrolex Red) provides a sufficiently high Stokes shift to minimize reabsorption effects within the secondary emitters and allows the use of quenching-based applications. In the theoretical chapter the focus lies on a comparison of geometrical with electromagnetic waveguide optics, giving an overview of the concept of modes. While summarizing different coupling mechanisms a more detailed chapter explains fluorescence and the radiation characteristics of dipoles near interfaces. As a foundation for the experimental section ray tracing simulations were done to investigate the radiation of a point source inside a planar waveguide model. A numerical analysis with the software package Mathematica presents the profile of modes in such a structure. In the experimental part a planar waveguide system (similar to [1]) consisting of a polydimethylsiloxane cladding with a polystyrene core on a flexible foil is used. The basic arrangement of the aspired sensor system can be seen in Fig. 1.1. Light from an organic light emitting diode excites fluorescent molecules, which couple light into a high refractive index core material. After being guided along the waveguide it is coupled out by scatterers to be detected by an organic photodiode. The gas permeability of the used materials allows the usage of indicators, which could be embedded in the core in future sensor applications. Different techniques to deposite the fluorescent molecules inside or on top of the core material are presented. To couple light out of the waveguide edge-coupling is compared to scattering by titanium oxide nanoparticles. Futhermore the influence of the thickness of the waveguiding layer and the intensity of the excitation source is investigated. An outlook on possible applications in the future concludes the work. As the topic of this thesis is related to the sensors presented in the ISOTEC research cluster [2], the concept includes an organic light emitting diode and photodiode even though later on inorganic components are used.

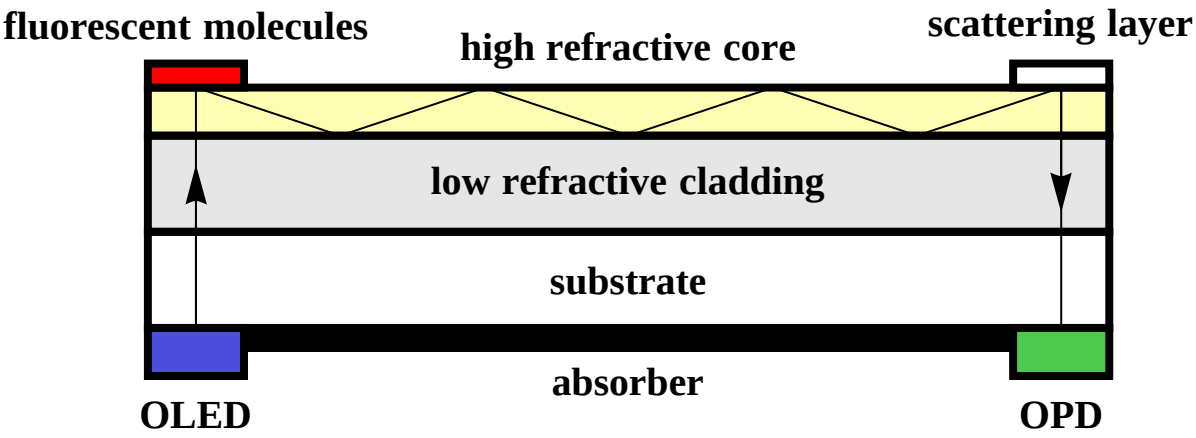

Figure 1.1: The basic planar sensor concept includes an organic light emitting diode, which excites fluorescent molecules either located on top of or inside the waveguide layer. The guided light is coupled out by scatterers, which redirect the light to an organic photodiode detector. The absorbing material suppresses modes travelling through cladding and substrate. [2]

Chapter 2

Theory

This chapter provides an overview of waveguide theory, comparing two different theoretical electromagnetic approaches with the geometric optical viewpoint. In addition to an explanation resulting from the wave equation and the Maxwell equations, the interference inside a planar waveguide leads to the concept of modes. The result of these explanations is the transcendental equation for a planar waveguide, which will be used in the simulation chapter to calculate the profile of optical modes. A discussion of the basic properties of modes will be followed by an examination of different coupling mechanisms, specially focusing on dipole radiation near interfaces, resonance energy transfer and fluorescent molecules. A resonance energy transfer system, consisting of two different Macrolex dyes, is used in the experimental part to couple light into the waveguide.

2.1 Waveguide optics

When dealing with integrated optical waveguide sensors, it is first nescessary to define the term waveguide itself. A waveguide is a structure in which electromagnetic waves can be bound in a way that they can travel along a given path from one point in space to another. The first thought is to use mirrors to reflect rays or an array of lenses to guide the light along a certain path. Lenses reflect a part of the incoming light, anti-reflection coated devices are very expensive while mirrors on the other hand absorb a part of it. Another way is to confine the electromagnetic waves by conductive materials as it is done by coaxial-cables. To avoid losses due to the skin effect at the boundary walls, which dominate at high frequencies (above around 1 GHz), it is obvious to approach the concept of dielectric waveguides and total internal reflection. Waveguides which are used in the visible spectrum are called optical waveguides.

Optical waveguides can be classified by their assembly into fibre waveguides and integrated optical waveguides. Basically both of them consist of an outer material with a

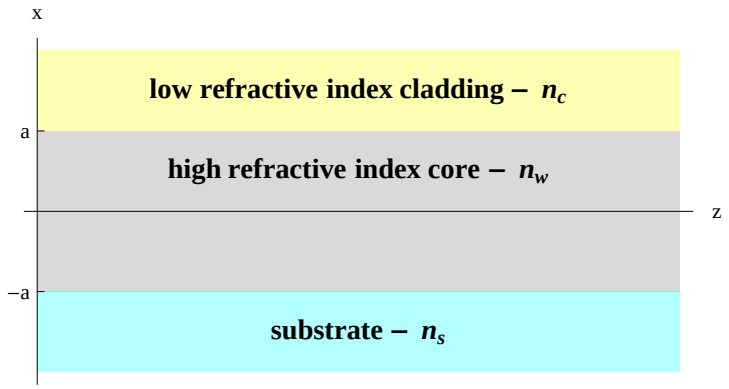

Figure 2.1: The basic assembly of a planar waveguide. A high refractive index core material is embedded between two lower refractive index materials, the substrate and the cladding. The core has the thickness 2a, the x-axis and the z-axis lie in the plane of projection, the y-axis is orthogonal to the plane of projection.

lower refractive index (cladding) and of an inner material with a higher refractive index (core). In Fig. 2.1 one of the outer materials is the substrate, on which the waveguide is assembled. There are two possible approaches to deal with optical waveguiding in dielectric materials. First we take a look at geometric optics and then we will continue with the electromagnetic viewpoint. In the electromagnetic viewpoint we will investigate a description resulting from the Maxwell equations and a model using interference. Both electromagnetic viewpoints will lead to the concept of modes. [3]

2.1.1 Geometrical optics

The basic postulates in geometrical optics are

- Light travels as rays, which are emitted from light sources and can be detected by optical detectors.
- Optical media are characterized by the refractive index, which is defined by $n = \frac{c_0}{c}$. The time needed to travel a distance d is $\frac{d}{c} = \frac{nd}{c_0}$, where c_0 is the speed of light in vacuum and c the corresponding speed in a medium with refractive index n.
- nd is called optical waylength and - if the medium is inhomogenous - is defined by

$$optical\,waylength = \int_A^B n(r)\,ds \tag{2.1}$$

- Fermat's principle: A light ray travels between two points A and B in a way that the travel time reaches an extremum compared to all other possible ways [4]. If it is a minimum Fermat's princible turns to: Light takes the path which needs the shortest amount of time. The exact mathematical formulation uses the variation of the optical waylength.

$$\delta \int_A^B n(\mathbf{r})\, ds = 0 \tag{2.2}$$

Fermat's principle is for example used to investigate effects in inhomogenous media. With the help of calculus of variation Eq. (2.2) can be written as Eq. (2.3). [5, 6]

$$\frac{d}{ds}(n\frac{d\mathbf{r}}{ds}) = \nabla n \tag{2.3}$$

We now investigate the effects of a ray of light that hits an interface of two different dielectrics with a refractive index difference $\Delta n = n_1 - n_2$. The basis for the geometric optical viewpoint are the law of reflection and Snell's law.

$$\alpha = \alpha' \tag{2.4}$$

$$n_1 \sin\alpha = n_2 \sin\beta \tag{2.5}$$

Depending on the angle α (to the interface normal) of the incident ray, one part of the ray is reflected and the other transmitted at an angle β. The transmitted ray is refracted in a way that the optical waylength in each direction is minimized ($n\frac{ds}{dx} = 0$). Based on the postulates above the waylength in the optical thinner material is increased on the cost of the waylength in the optical thicker material. In Fig. 2.2 the chosen way to travel between A and B ($n_1 > n_2$) is therefore not the direct one. The waylength in the higher refractive material n_1 is reduced by travelling a shorter distance while on the other hand in the lower refractive material the waylength is increased compared to the direct way.

With the help of the wave theory of light and the Fresnel coefficients it is possible to calculate the intensity of the reflected and transmitted ray. At an angle of $\alpha = 0°$ 4% of the incoming ray is reflected. Let us assume light is propagating from A to B (from the higher refractive index to the lower refractive index material). The larger α gets the larger the fraction which is reflected reaching a maximum of 100% at an angle which is defined by the two materials. This angle is called critical angle and calculated by setting $\beta = 90°$ in Eq. (2.5). [3]

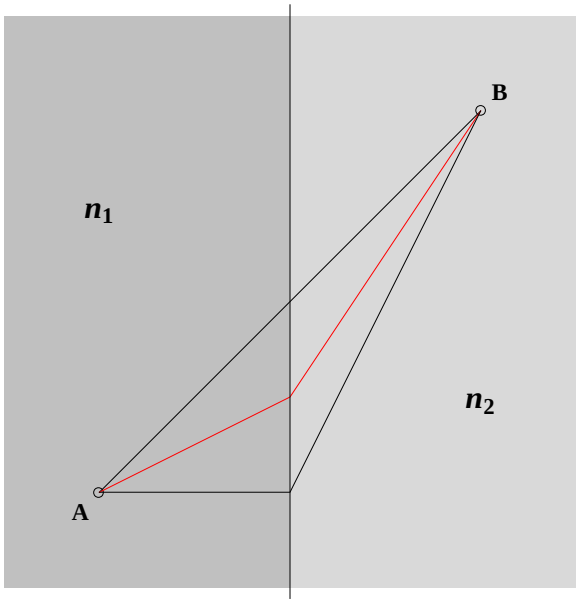

Figure 2.2: Fermat's principle of refraction for light propagating from a higher to a lower index material or vice versa ($n_1 > n_2$). Light chooses the path which needs the shortest time as indicated in red.

$$\alpha_{crit} = \arcsin \frac{n_2}{n_1} \tag{2.6}$$

For rays with an incident angle larger than the critical angle 100% of the ray is reflected. Light that travels at an angle beyond α_{crit} in a medium with a higher refractive index than the surrounding material and ís trapped inside a waveguide, if there is a second low refractive index material which reflects the ray back. For formulae on Fresnel coefficients see [7].

Step-index and gradient-index waveguides

An idealized waveguide, in which the refractive index of the core is not varying laterally and does not show any attenuation, is called step-index waveguide and shows a refractive index profile as in figure Fig. 2.3a. While flexing the waveguide the angle of the incident ray now has to be based on the tangent to the interface instead of the interface itself (as demonstrated in Fig. 2.4). For higher bending radii this angle is smaller than α_{crit} leading to losses because part of the light leaves the system. Rays with a larger travelling angle have a lower probability of leaving the system.

If the refractive index in the core material is not constant but varies laterally the wave-

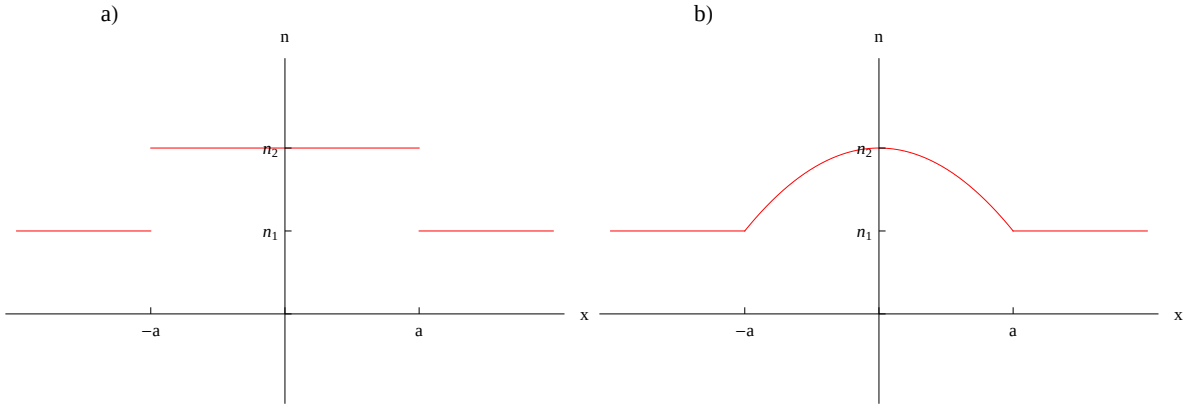

Figure 2.3: The difference between a step index a) and a gradient index waveguide b). While a step index waveguide shows a jump discontinuity at an interface, in a gradient index waveguide the refractive index is decreasing gradually from n_2 at the center to a constant value n_1 for $x \geq a$ and $x \leq -a$.

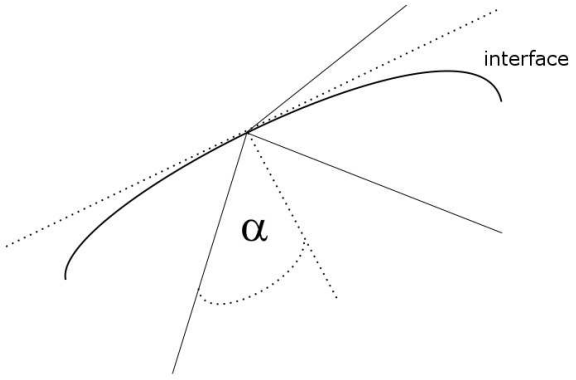

Figure 2.4: When bending a waveguide the angle of a ray has to be evaluated with respect to the tangent of the interface normal, which can reduce the amout of light that can propagate inside the waveguide.

guide is called gradient-index waveguide. This case is exemplarily sketched in Fig. 2.3b. The refractive index decreases gradually, given by a profile function f(x), from a maximum value n_1 at the center of the waveguide to a constant value n_2 outside the interface. This leads to a curved path of light between the two interfaces. A special distribution is given by a parabolic refractive index distribution. These "lenses" are cylindrical devices and are known by the trademark SELFOC [8]. The refractive index varies in x-direction but is constant in the y- and z-direction. The axis orientation is given according to Fig. 2.1.

$$n^2(x) = n_1^2\,(1 - \bar{\alpha}^2 x^2) \tag{2.7}$$

Most of the time $\bar{\alpha}$ is chosen very small. If we assume that the ray is travelling close to the z-axis ($ds = dz$) Eq. (2.3) is reduced to

$$\frac{d^2x}{dz^2} = \frac{1}{n(x)}\frac{dn(x)}{dx} \tag{2.8}$$

Using Eqs. (2.7) and (2.8) leads to a differential equation

$$\frac{d^2x}{dz^2} = -\bar{\alpha}^2 x \tag{2.9}$$

which gives, together with the boundary conditions $x(0) = x_0$ and $\frac{dx}{dz} = \theta_0$, the solution

$$x(z) = x_0 \cos\bar{\alpha}z + \frac{\theta_0}{\bar{\alpha}} \sin\bar{\alpha}z \tag{2.10}$$

Starting at a random point x_0 inside the waveguide, the light chooses a sine-cosine curve for every angle, even if the starting angle is 0° (outside of the center $x_0 = 0$). Special about SELFOC-lenses is that α is chosen so small that all rays with different angles and starting points meet again in one point on the axis after a period of $\frac{\pi}{\bar{\alpha}}$. The amplitude of the sine motion however changes for different starting coordinates.

The concept of step-index and gradient-index waveguides can be widend to fibre waveguides. In gradient-index fibre waveguides the guided wave now has the chance to travel around a helix shaped curve. [3, 6]

Matrix optics

A useful approach in geometrical optics which can also be applied for refraction, is the concept of matrix optics. A ray of light interacting with an optical system which is rotationally symmetric around the z-axis can be characterized by its distance from the z-axis and its propagation angle θ. After interaction with the optical system, the coordinates are changed from (z_1, θ_1) to (z_2, θ_2). Each of the "new" coordinates depends on both of the "old" coordinates. So they can be written in a matrix notation where the matrix is called transfer matrix.

$$\begin{bmatrix} z_2 \\ \theta_2 \end{bmatrix} = \begin{bmatrix} A & B \\ C & D \end{bmatrix} \begin{bmatrix} z_1 \\ \theta_1 \end{bmatrix} \tag{2.11}$$

For refraction at an interface with the two refractive indices n_1 and n_2 the paraxial approximation is used to replace Snell's law. This means that the angle to the optical axis stays small ($\sin\theta = \theta$), leading to the transfer matrix given in Eq. (2.12).

$$M = \begin{bmatrix} 1 & 0 \\ 0 & \frac{n_1}{n_2} \end{bmatrix} \tag{2.12}$$

In the same way transfer matrices can be definied for lenses or mirrors. The big advantage of this viewpoint is that coupled systems can be easily studied by matrix multiplication. Matrix optics is, for example, used by ray-tracing simulation programs. [5, 6]

Limitations of the geometrical optics

By dealing with light only in the geometric optical viewpoint we might end up in wrong conclusions. The end face of the waveguide is not uniformly bright. What we observe are light distributions, which can be explained by the concept of modes. Some phenomena such as evanescent waves are simply not explainable with geometrical optics. It is thus necessary to expand our theoretical discussion to eletromagnetic waves. [3]

2.1.2 Electromagnetic optics

Basics

Geometrical optics is included in the theory of wave optics in the limit $\lambda \to 0$. The mathematical description follows the wave equation, a differential equation of second order, where $\mathbf{u}$ is a function of time and the three space coordinates $\mathbf{u} = \mathbf{u}(t, x, y, z)$.

$$\nabla^2 \mathbf{u} - \frac{1}{c^2} \frac{\partial^2 \mathbf{u}}{\partial t^2} = 0 \tag{2.13}$$

The complex solution of the wave equation for monochromatic waves constists of a time dependent part and a complex amplitude $U(\mathbf{r})$ which is independent of time.

$$U(\mathbf{r}, t) = U(\mathbf{r})\, exp(i2\pi\nu t) = U(\mathbf{r})\, exp(i\omega t) \tag{2.14}$$

$$U(\mathbf{r}) = a(\mathbf{r})\, exp(i\phi\mathbf{r}) \tag{2.15}$$

Equation (2.14) can be considered in a complex diagram where $a(\mathbf{r})$ represents the length of the vector and ϕ the phase of the wave. Both are included in the complex amplitude $U(\mathbf{r})$. Using $\omega = 2\pi\nu$ the rotation of the vector - the time dependence of the wave - is described. The real part of Eq. (2.14) describes the actual wave.

The complex amplitude follows the Helmholtz equation.

$$\nabla^2 U + k^2 U = 0 \tag{2.16}$$

where k is the wavenumber

$$k = \frac{2\pi\nu}{c} = \frac{\omega}{c} \tag{2.17}$$

Of spectial importance concerning waveguides are plane waves. A solution of the Helmholtz equation for a plane wave is

$$U(\mathbf{r}) = A\, exp(i\mathbf{kr}) = A\, exp(i(k_x x + k_y y + k_z z)). \tag{2.18}$$

The area with constant phase (wave fronts) are in this case parallel planes which are normal to the wavevector $\mathbf{k}$. The wavenumber is given by $k^2 = k_x^2 + k_y^2 + k_z^2$ and the distance between the wavefronts is the wavelength λ. [6]

$$\lambda = \frac{c}{\nu} = \frac{2\pi}{k} \tag{2.19}$$

Electromagnetic waves in a dielectric slab waveguide

A dielectric slab waveguide consists of three cuboid voluminae, a high refractive index material, which is embedded between two lower refractive index materials. As we are now interested in waves in different media, the Maxwell equations have to be taken into account if we want to describe the conditions inside a dielectric slab waveguide.

$$\nabla \times \mathbf{E} = -\frac{\partial \mathbf{B}}{\partial t} \tag{2.20}$$

$$\nabla \times \mathbf{H} = \frac{\partial \mathbf{D}}{\partial t} + \mathbf{j} \tag{2.21}$$

$$\nabla \cdot \mathbf{D} = \rho \tag{2.22}$$

$$\nabla \cdot \mathbf{B} = 0 \tag{2.23}$$

To observe the behavior of electromagnetic fields in matter we need the constitutive relations where ϵ and μ are tensorial quantities.

$$\mathbf{D} = \epsilon_0 \epsilon_r \mathbf{E} \tag{2.24}$$

$$\mathbf{D} = \epsilon_0 \mathbf{E} + \mathbf{P} \tag{2.25}$$

$$\mathbf{P} = \epsilon_0 \chi_e \mathbf{E} \tag{2.26}$$

$$\mathbf{B} = \mu_0 \mu_r \mathbf{H} \tag{2.27}$$

$$\mathbf{H} = \mu_0^{-1} \mathbf{B} - \mathbf{M} \tag{2.28}$$

$$\mathbf{M} = \chi_m \mathbf{H} \tag{2.29}$$

Electromagnetic waves are described as a solution of the following version of Eq. (2.13) where the wavenumer now is defined by $k = \omega\sqrt{\mu\epsilon} = \frac{\omega}{c}$.

$$\nabla^2 \mathbf{E} - \mu\epsilon \frac{\partial^2 \mathbf{E}}{\partial t^2} = 0 \tag{2.30}$$

Table 2.1: Important quantities with their symbols concerning the Maxwell equations.

Symbol	Quantity
E	electric field
H	magnetizing field
D	electric displacement field
B	magnetic flux density
j	electric current density
ρ	charge density
P	polarization
M	magnetization
ϵ_0	vacuum permittivity
ϵ_r	relative permittivity
μ_0	vacuum permeability
μ_r	relative permeability
χ_e	electric susceptibility
χ_m	magnetic susceptibility

Phase velocity and group velocity

The time after which a wave reaches the same phase again defines, together with the distance covered, the phase velocity. The phase speed is connected with the wavevector k, which is also dependent on the angular frequency ω.

$$v_{ph} = \frac{\omega}{k} \tag{2.31}$$

When speaking of a wave packet it is necessary to define the group velocity, which covers the movement of the packet as a whole. Together with Eq. (2.31) the speed of the envelope is now given by

$$v_g = \frac{d\omega}{dk} = v_{ph} + k\frac{dv_{ph}}{dk} \tag{2.32}$$

This leads to the fact that the phase and the group velocity differ from each other if the phase velocity is dependent on the wavevector. [9]

The infinite slab waveguide

Starting point now is the simplest waveguide assembly. The infinite slab waveguide has a higher refractive material n_w (core, waveguide) in between two lower index materials n_s (substrate) and n_c (cladding) as shown in Fig. 2.1. The propagation direction is chosen to be the z-direction. The x-direction points upwards, the y-direction is perpendicular to the plane of projection and $n_w > n_s > n_c$. Note that from now on the point of origin lies *between* core and cladding (at the interface) and the core has the thickness d=2a. We choose transverse electric polarization where the electric field has no (longitudinal) component in the propagation direction z and is transverse to the plane defined by k and the interface normal (plane of incidence). Because of the constancy of the angular frequency in media ($k = \frac{\omega_0}{c}$ and $k_0 = \frac{\omega_0}{c_0}$ which leads to $n_j = \frac{c_0}{c} = \frac{k}{k_0}$) it is possible to write Eq. (2.30) as an equation which describes the electric field oriented in the y-direction.

$$\nabla^2 E_y + k^2 E_y = \nabla^2 E_y + k_0^2 n_j^2 E_y = 0 \tag{2.33}$$

To describe the electric field we use the following ansatz Eq. (2.34) leaving the time dependence from Eq. (2.18) behind because we are just interested in the shape of the modes. The electric field does not depend on the y-coordinate ($\frac{dE_y}{dy} = 0$ and $\frac{d^2E_y}{dy^2} = 0$) because the waveguide is infinite in that direction. The propagation constant β describes the modulation the wave undergoes in z-direction.

$$E_y(x, z) = E_y(x)e^{-i\beta z} \tag{2.34}$$

Putting Eq. (2.34) into Eq. (2.33) gives us the differential equation for $E_y(x)$ by differentiation with respect to x (first term in Eq. (2.35)) and z (second term in Eq. (2.35)).

$$\frac{\partial^2 E_y(x)}{\partial x^2} + (-\beta^2 + k_0^2 n_j^2)E_y(x) = 0 \tag{2.35}$$

The differential equation Eq. (2.35), which in our case results from the basic wave equation Eq. (2.30), can also be found directly by plugging the ansatz Eq. (2.18) for a plane wave in z-direction into the Maxwell equations Eq. (2.20) and Eq. (2.21). This approach, together with the treatment of a rectagular waveguide (non infinite in y- and z-direction), can be found in [10].

The solution of Eq. (2.35) is dependent on the electric field at $x = 0$ times an exponential function.

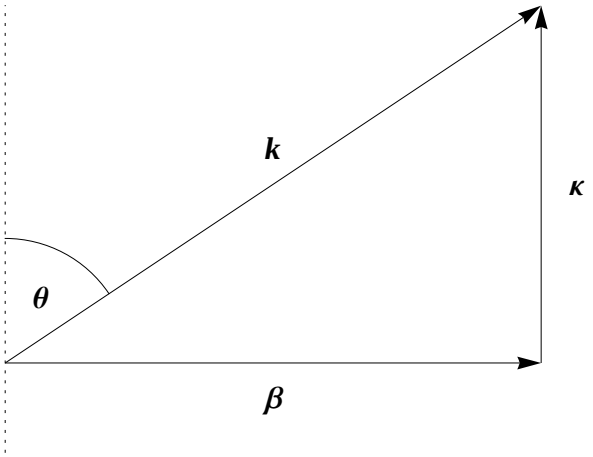

Figure 2.5: The wavevector **k** is composed of the longitudinal component β and the transversal component κ, which form a right angle triangle.

$$E_y(x) = E_0 e^{\pm\sqrt{\beta^2 - k_0^2 n_j^2}x} \tag{2.36}$$

Looking at the term under the root the solution can be either oscillating or exponentially decaying. In the case of $\beta > k_0 n_j$, $\gamma = \sqrt{\beta^2 - k_0^2 n_j^2}$ is called the attenuation coefficient and the solution is described by

$$E_y(x) = e^{-\gamma x} \tag{2.37}$$

If $\beta < k_0 n_j$, $\kappa = \sqrt{k_0^2 n_j^2 - \beta^2}$ is the transverse wavevector and the solution is

$$E_y(x) = e^{\pm i\kappa x} \tag{2.38}$$

In the oscillating case the the wavevector consists of two components, the longitudinal component β pointing into the z-direction and the transverse component pointing into the x-direction. Those two components are defined by the angle θ of **k** relative to the interface, as illustratet in Fig. 2.5.

Three cases of wave propagation - evanescent waves

If the system consists of three layers with different refractive indices, β can now lie in different ranges with respect to the product $k_0 n_j$. In the first case $\beta < k_0 n_c$, light is

refracted at both interfaces when passing through the system. The solution is oscillating in all three areas. If $k_0 n_c < \beta < k_0 n_s$, the solution is oscillating in the substrate and the waveguide, but exponentially decaying in the cladding material. This solution corresponds to refraction at the substrate-core interface and total reflection at the cladding-core interface. Finally, $\beta > k_0 n_s$ means that the wave is now captured inside the waveguide being totally reflected at both interfaces.

The solution of the Eigenvalue equation

When searching for allowed values of β, κ and γ - using the third solution with an oscillating part in between two exponentially decaying parts - it is necessary to link the three different parts with each other. The boundary conditions which connect the areas are

- The tangential component of E is continuous at $x = 0$ and $x = -d$
- The tangential component of H is continuous $x = 0$ and $x = -d$

Transforming the continuity of H with the Maxwell equation Eq. (2.20) to a condition for the continuity of $\frac{\partial E_y}{\partial x}$ makes it possible to give a solution for the three areas.

$$E_y = Ae^{-\gamma_c x} \tag{2.39}$$

$$E_y = A[\cos \kappa_w x - \frac{\gamma_c}{\kappa_w} \sin \kappa_w x] \tag{2.40}$$

$$E_y = A[\cos \kappa_w d - \frac{\gamma_c}{\kappa_w} \sin \kappa_w d] e^{\gamma_s (x+d)} \tag{2.41}$$

The Eqs. (2.39), (2.40) and (2.41) are valid for the ranges $x > 0$, $-d < x < 0$ and $x < -d$. After using the continuity of $\frac{\partial E_y}{\partial x}$ at $x = -d$ we arrive at the transcendental Eigenvalue equation for κ_w.

$$tan(h\kappa_w) = \frac{\gamma_c + \gamma_s}{\kappa_w [1 - \frac{\gamma_c \gamma_s}{\kappa_w^2}]} \tag{2.42}$$

It is now possible to solve this equation graphically or numerically. When we look at the graphical way to solve Eq. (2.42) we have to find the intersection points of the curves given by the left and the right hand side expressions of this equation. Each solution for κ_w leads to unique values of γ_c, γ_s and β. It is important to notice that κ_w is not continuous. Each of the discrete values of κ_w corresponds to a specific curve shape in

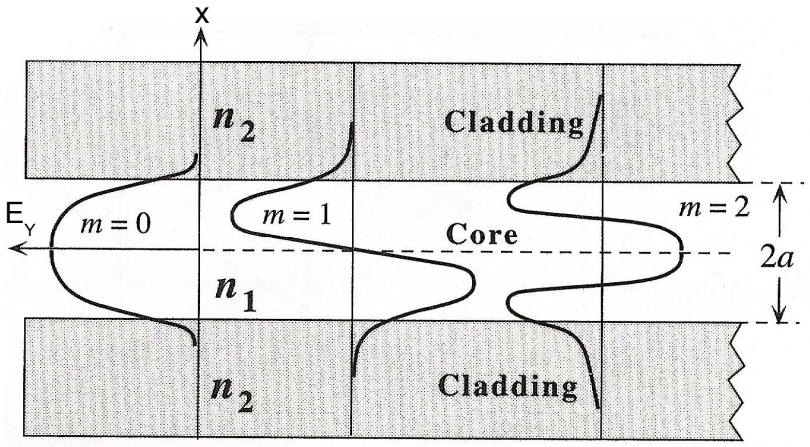

Figure 2.6: Basic shape of the first three modes inside a core material with the thickness 2a. The amplitudes were normalized for easier comparison. [12]

the three materials of the waveguide. Those solutions are referred to as different modes. It is now noticable that even if the wave is trapped inside the waveguide there is still a wave in the low refractive parts. This wave is called evanescent wave and is very important for sensor applications. A detailed numerical analysis together with electric field patterns of modes will be presented in Sec. 3.1. [11]

Alternative concept of modes using interference

Another approach to achieve the concept of modes is by analyzing interference inside the waveguide. A plane wave travelling at an angle α with a wavenumber k is totally reflected at each of the interfaces touching the high refractive core material. When reflected the wave undergoes a phase change of ϕ. Starting at a point P, after being reflected at Q and R the wave interferes with itself. To make constructive interference possible the phase difference between the two waves has to be an integer multiple of 2π. Following Fig. 2.7 the phase difference between P and R has to be

$$\Delta\Phi(PR) = k(PQ + QR) - 2\phi = 2\pi m \tag{2.43}$$

Basic geometry yields $PQ + QR = 2d\cos\theta$ where d is the thickness of the core material in x-direction. This leads to the waveguide condition Eq. (2.44).

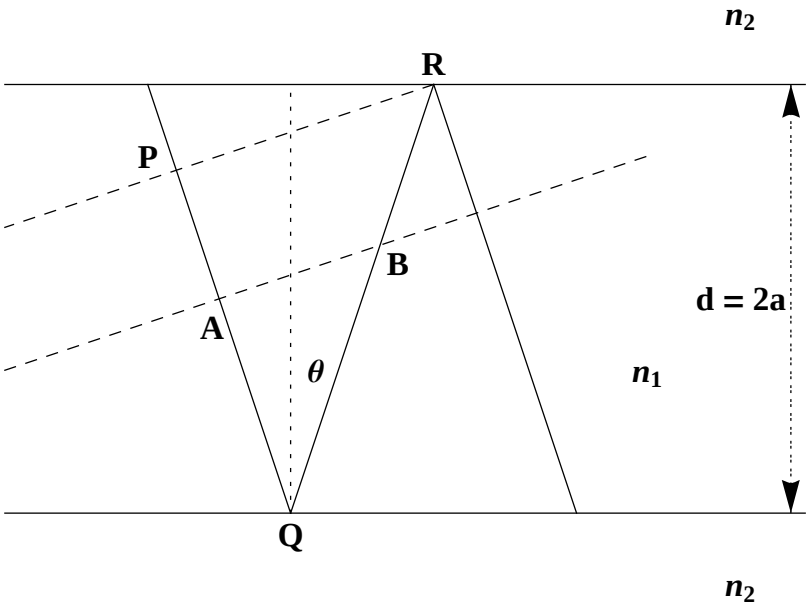

Figure 2.7: Interference inside a waveguide of thickness 2a. After two reflections a wave starting at a point P interferes with itself at the point P. At each reflection the wave undergoes a phase shift ϕ_m, which is dependent on the polarization.

$$2d\,k\,cos\theta_m - 2\phi_m = 2\pi m,\ m = 0, 1, 2, 3... \tag{2.44}$$

The phase shift ϕ_m is also dependent on the incident angle θ_m, where the index m stands for the discrete solutions. The phase difference Φ_m of a wave that interferes with the reflection of itself at any point B with the coordinate x inside the waveguide is given in Eq. (2.45). The origin of the x-coordinate is in the center of the waveguide, a is the distance between the interface and the center, $d = 2a$.

$$\Phi_m(x) = m\pi - \frac{x}{a}(m\pi + \phi_m) \tag{2.45}$$

The solution now results from interfering the two phase shifted waves, travelling under the same angle in different x-directions.

$$E_1(x, z, t) = E_0 \cos(\omega t - \beta_m z + \kappa_m x + \Phi_m) \tag{2.46}$$

$$E_2(x, z, t) = E_0 \cos(\omega t - \beta_m z - \kappa_m x) \tag{2.47}$$

The values β_m and κ_m again represent the longitudinal and transversal wavevector component. Adding Eq. (2.46) and (2.47) now gives the final result

$$E(x,z,t) = 2E_0 \cos(\kappa_m x + \frac{1}{2}\Phi_m)\cos(\omega t - \beta_m z + \frac{1}{2}\Phi_m) \tag{2.48}$$

The light is distributed as a standing wave along the x-direction as there is no time dependence in the first cosine term. It is travelling with the propagation constant β_m in z-direction. Similar to the previous chapter we assume the wave as transverse electric so the electric field points in the y-direction. Note that even if $x = a$ (at the interface) the wave is not equal to zero. This leads us again the phenomenon of evanescent waves.

The phase change ϕ upon total reflection is dependent on the polarization as well. In the transverse electrical case ϕ is defined by

$$\tan(\frac{1}{2}\phi_m) = \frac{\sqrt{\sin^2\theta_m - (\frac{n_2}{n_1})^2}}{\cos\theta_m} \tag{2.49}$$

For each waveguide configuration and mode number there are unique values for κ_m and β_m, which can be calculated by plugging the waveguide condition Eq. (2.44) into Eq. (2.49).

$$\tan(ak\cos\theta_m - m\frac{\pi}{2}) = \frac{\sqrt{\sin^2\theta_m - (\frac{n_2}{n_1})^2}}{\cos\theta_m} \tag{2.50}$$

Using the solution for β_m from Eq. (2.50) in Eq. (2.48) makes it again possible to draw the different modes. [12, 13]

Properties of modes

Modes are classified after their mode number m starting with $m = 0$ for the lowest mode. Lower modes correspond to larger values of θ_m (relative to the interface normal). The $m = 0$ mode has the angle closest to 90° (to the interface normal) and has no electric field nodes along the x-axes. For higher modes the mode number also equals the number of nodes. If the refractive index of the substrate and the cladding are the same (symmetric waveguide), modes with an even mode number are even functions, odd mode numbers correspond to odd functions. The mode m=4 in a symmetric waveguide has for example four nodes and is symmetric. The higher the refractive index difference between substrate and cladding the stronger the asymmetry gets.

The wave equation Eq. (2.44) so far allowes angles from 0-90°. To be able to determine the number of modes which are allowed to travel inside the waveguide, we have to take into account that there is a critical angle for total internal reflection. Some higher modes (with lower angles) will not be able to propagate. This leads to a cutoff condition [12] for propagating modes

$$m \leq \frac{2V - \phi}{\pi} \tag{2.51}$$

where V is the V-number or normalized thickness and m can now be every integer number smaller than the term on the right hand side.

$$V = \frac{2\pi a}{\lambda}\sqrt{n_1^2 - n_2^2} \tag{2.52}$$

For multimode waveguides V is bigger than 1, the phase difference ϕ upon total reflection cannot be larger than π, so $\frac{\phi}{\pi}$ can not extend 1. With those two assumptions we can, including the m=0 mode, express Eq. (2.51) as a function of the number of modes M allowed to propagate in a waveguide.

$$M = Int(\frac{2V}{\pi}) + 1 \tag{2.53}$$

For a given waveguide structure on the other hand it would be interesting to find out which wavelength leads to the situation that only one mode, $m = 0$, is able to propagate. For $m = 0$, θ_m is almost $\frac{\pi}{2}$ and the phaseshift ϕ is reaching π. This means that from Eq. (2.51) we get the condition

$$V = \frac{\pi}{2} \tag{2.54}$$

If V reaches a value below $\frac{\pi}{2}$ the only mode which can propagate is $m = 0$. For a given waveguide thickness a and refractive indices n_1 and n_2 we can now calculate a cutoff wavelength λ_{cut} above which just one mode can propagate. In a 10 μm waveguide (a=5 μm) with the refractive indices ($n_1 = 1.59$ and $n_2 = 1.42$) the cutoff wavelength would lie around λ_{cut}=14.3 μm.

The higher the mode index the further the evanescent waves reach inside the cladding material. Looking at Eq. (2.52) gives the following results: The larger the V-number the higher the number of allowed modes is. A larger V-number can be acchieved by

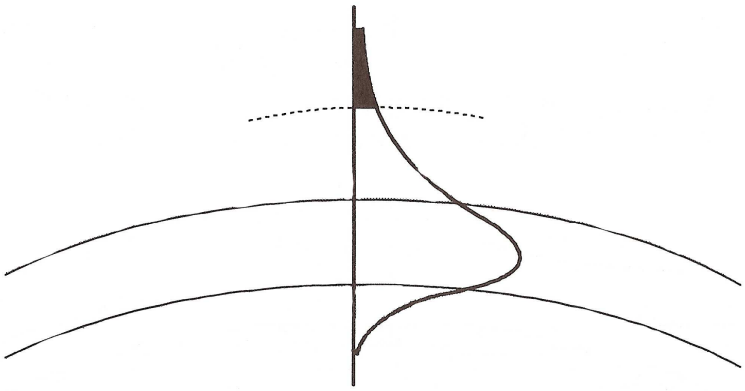

Figure 2.8: From the electromagnetic viewpoint when bending a waveguide the outer part of the wave should travel faster. As this is not allowed the part of the evanescent wave highlighted in black leaves the waveguide. [3]

increasing the refractive index difference between the two media, by using a thicker waveguide or decreasing the excitation wavelength.

Evanescent waves lead to a wealth of phenomena. A ray a of light can, for example, even though it is totally reflected at an interface, pass through a small gap between two media, provided that the evanescent wave reaches far enough. This effect is analog to quantum mechanics referred to as optical tunneling or frustrated total reflection. Another important conclusion is that the totally reflected wave interacts with the surrounding media via the evanescent wave, which is used for sensor applications. Furthermore you can also explain the loss which occurs while bending the waveguide. The outer part of the wave should travel at a faster velocity than the inner part to keep up with the wave. This is not allowed, so a part of the wave leaves the system. The higher the mode the bigger the bending loss is. [3, 12]

Modal dispersion

Each of the modes travels at a specific velocity through the waveguide. Lower modes, which actually have a longer waylength through the system, travel at a higher velocity even if the excitation source has a constant frequency. Here the difference to the geometric optical viewpoint can be seen. This fact would violate Fermat's principle. The reason for this is because higher modes reach further into the cladding material where the refractive index is smaller. It is possible to calculate dispersion diagrams which show the frequency ω over the longitudinal component β_m. In those diagrams the slope of the curves corresponds to the group velocity v_g. The curves happen to be between two lines given by $\frac{c}{n_1}$ and $\frac{c}{n_2}$. In a multimode waveguide the group velocity of the funda-

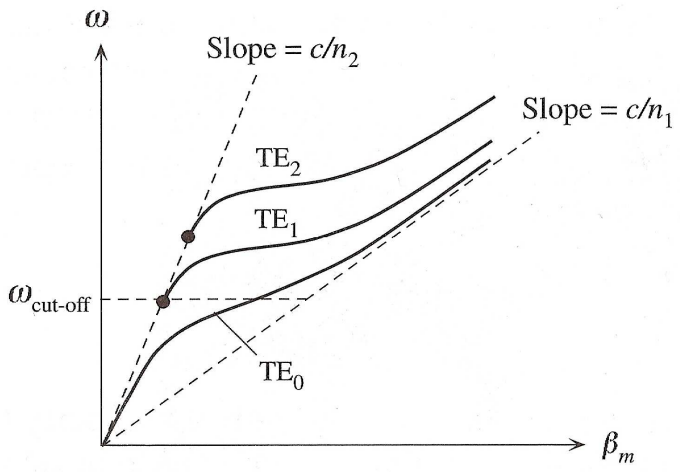

Figure 2.9: The group velocity of different modes can be approximated using phase diagrams, where the frequency of the wave is plotted over the longitudinal wavevector for each mode. The tangent of the curves gives the group velocity v_g. [12]

mental mode (m=0) lies close to $\frac{c}{n_1}$ while the one of the highest mode reaches $\frac{c}{n_2}$. The intersection of a constant ω with those curves defines the allowed modes.

$$\frac{c}{n_1} \leq v_g \leq \frac{c}{n_2} \tag{2.55}$$

A short pulse of light disperges in the waveguide. Note that the travelling velocity is as well dependent on the polarization.

Intramodal dispersion

Larger wavelengths (at a constant mode number) reach further into the cladding material. Because there is no perfect monochromatic source there will always be a so called waveguide dispersion even if the different wavelengths have the same mode number. A second source of dispersion is the dependence of the refractive index on the wavelength, which leads to material dispersion. Those two kinds of dispersions together are called intramodal dispersion. We note that to avoid dispersion in telecommunication single mode waveguides are used. [12]

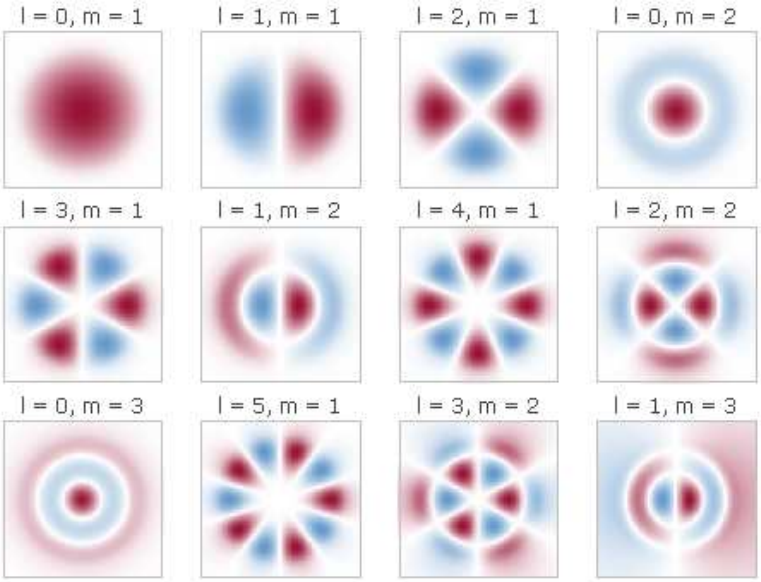

Figure 2.10: Modes in an optical fibre waveguide. The number of maxima of the electric field vector in the radial and angular direction are described by the parameters l and m. [14]

2.1.3 Fibre waveguide

The concept of modes can be extended to fibre waveguides. As discussed before, rays can not only travel axially but also have a chance to take a helical path. The longitunal component β_m is then dependent on two parameters m and l (β_{ml}) as the interface now is cylindrical. These two parameters describe the shape of the modes. For low refractive index differences light is linearly polarized (meaning that E and H have no component in z-direction and are perpendicular to each other). When looking at the distribution of the electric field vector in the xy-plane we see that m gives us the number of maxima along the radial direction and $2l$ the number of maxima in the angular direction. The 2-1-mode, for example, consists of 4 spots with maxima at the same distance to the center. A detailed view on fibre waveguides can be found in [3, 12]. Figure 2.10 shows exemplarily the electric field amplitude for several guided modes in an optical fibre in the x-y-plane.

2.1.4 Numerical aperture

Considering the content of the next chapter the term numerical aperture must be introduced. The numerical aperture N_A in general defines the ability of an optical element to focus light. In this context we have to think of it the other way around as it describes

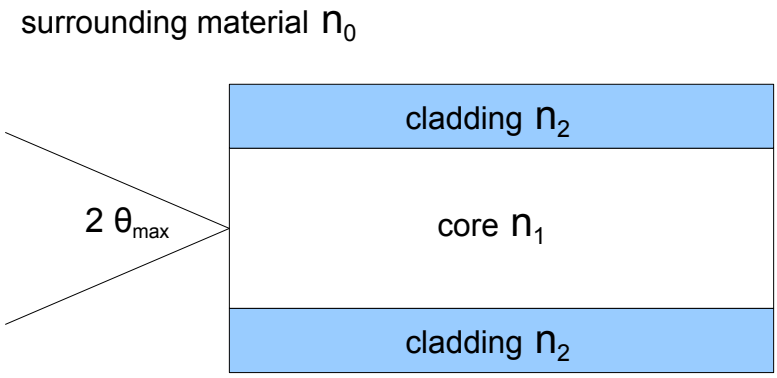

Figure 2.11: The numerical aperture defines the maximum angle θ_{max} of acceptance to guide light inside a wavguide.

an angle of acceptance for rays from outside to be trapped inside a waveguide. Let us assume a planar waveguide with a core material (n_1) in between two cladding materials (n_2). The whole waveguide is surrounded by a material with the refractive index n_0. If we illuminate the front face of the core material from outside, rays are refracted and will enter the waveguide. Some rays which enter have an angle beyond the critical angle relative to the core-cladding interface, are totally reflected and trapped inside the waveguide. The rest of the rays lies below the critical angle and leaves the waveguide either through the top or bottom cladding at the first encounter. For certain conditions it is possible to calculate the maximum angle of acceptance θ_{max} for which total reflection inside the waveguide is given in a symmetric waveguide (see Eq. (2.56) and Fig. 2.11). [12]

$$\sin\theta_{max} = \frac{\sqrt{n_1^2 - n_2^2}}{n_0} = \frac{N_A}{n_0} \tag{2.56}$$

If the outer material is air ($n = 1$), we can express the V-number (compare Eq. (2.52)) in terms of the numerical aperture as

$$V = \frac{2\pi a}{\lambda} N_A \tag{2.57}$$

2.2 Coupling mechanisms

After investigating the propragation of light inside a waveguide it is necessary to think of ways to couple light into and out of the waveguide. For sensor applications using evanescent waves the amount of light inside the waveguide should be as high as possible while the sensor structure should be cheap, reliable and compact. The following chapters give an overview of applicable coupling structures with a detailed focus on fluorescent molecules since they are used in the experimental section.

2.2.1 In-coupling

Depending on their orientation to the waveguide, coupling methods can be classified in transverse or longitudinal. End-fire coupling is a transverse coupling method while the rest of the described methods are longitudinal.

End-fire coupling

The numerical aperture has a limiting effect on the amount of light that can be coupled into a waveguide. The angle of the rays incident to the front face normal should be kept as low as possible for a given waveguide structure. Simply illuminating the front by a diffuse light source would be not effective, rather lenses to focus the rays should be used. This method is usually referred to as *direct*, *head-on* or *end-fire* coupling. As the dimensions of the typical sensor waveguides are usually around a few μm this method turns out to be complicated. In addition to that exact alignement is time consuming, high quality lenses are expensive and using light sources which are not included in the integrated sensor is generally not beneficial to the compactness of the sensor. [13]

Prism coupling

Let us assume we are concerned with a symmetrical waveguide. If we want to couple light transversally to the interface, we have to consider that any ray that enters at an angle α_1 lower than the critical angle is refracted to a lower angle α_2 and then emerges on the other side at the same angle $\alpha_3 = \alpha_1$. The goal now is to keep α_2 as large as possible to make total reflection possibe at the interface 2-3. This can be accomplished by a prism touching the interface 1-2. Incident rays first hit the inclined part of the prism and then - if the prisms consist of the same material as the waveguide - enter the waveguide without being refracted. By changing the prism side angle it is possible to

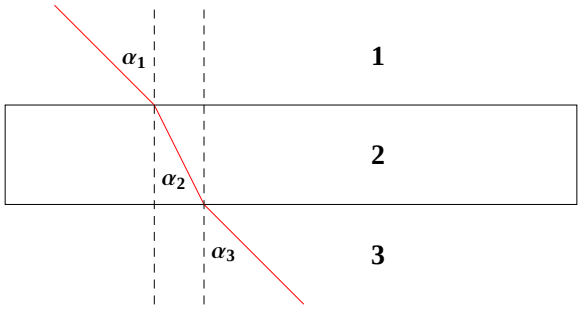

Figure 2.12: A ray which enters a waveguide a certain angle α_1 from a lower refractive material emerges at the same angle $\alpha_3 = \alpha_1$.

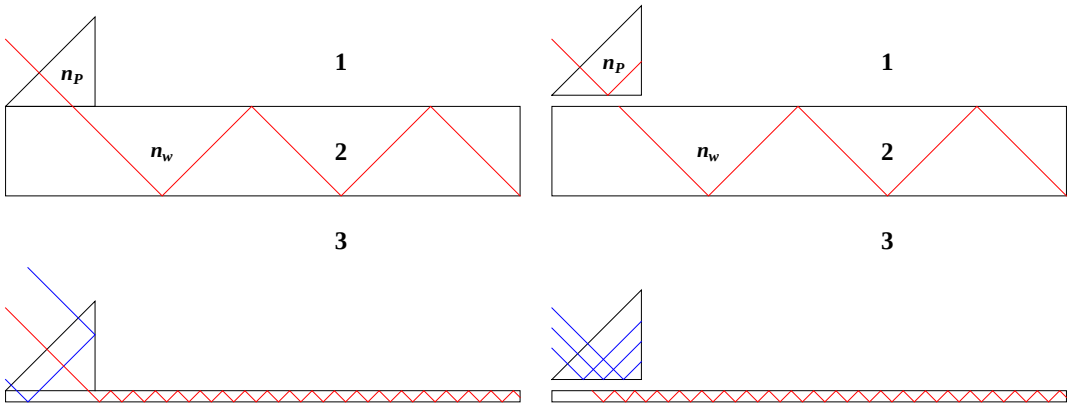

Figure 2.13: Four different arrangements based on prism coupling. On the left hand side the prism is touching the interface, on the right hand side a small gap is left between prism and waveguide to allow evanescent waves to couple in the waveguide.

allow rays with a larger incident angle to enter the waveguide. In any case the incident angle of the rays should be close to those of the allowed modes. The problem of this approach is that the smaller the thickness of the waveguide compared to the prism the more rays leave the waveguide through the prism again as evident from the the lower left sketch in Fig. 2.13. Ideally the prism should have a length in the order of the thickness of the waveguide or smaller and the width of the light bundle should also be of the same dimension. This leads to similar alignment problems as with end-fire coupling.

Another possibility when using prisms is employing evanescent waves. When there is a small gap between the prism and the waveguide itself, the incoming rays are now totally reflected at the plane parallel to the waveguide of the prism and excite evanescent waves which are - if they reach into the core - able to propagate there. The longitudial component of the wavevector β of the allowed modes in the waveguide has to be matched with the incident angle α of the rays following Eq. (2.58). In this equation k_P is the

wavenumber in the prism and k_0 the vacuum wavenumber, while n_P is the refractive index of the prism.

$$\beta = k_P \sin\alpha = k_0 n_P \sin\alpha \tag{2.58}$$

Waves which are coupled into the waveguide on the left side of the prism interfere with those on the right side. As demonstrated in the lower right picture of Fig. 2.13 the waves interfere to one standing wave pattern, which is highlighted in red. [15]

Grating coupling

Avoiding external optical devices, gratings give also an opportunity to couple light into waveguides. Gratings are usually etched or stamped into the top layer of the core-material. Using the grating equation it is possible to derive an equation which allows - for a given grating structure with the grating constant d - to determine the incident angle α for a mode with the logitudinal wave vector β to be excited.

$$\beta = k_C \sin\alpha - \frac{2\pi}{d} \tag{2.59}$$

Here k_C stands for the wavenumber in the cladding material. Important in Eq. (2.59) is that gratings with a higher grating constant couple light into the waveguide leading to higher values of β, which belong to modes of lower order.

Molecules (scattering, fluorescence)

Finally, another possibility of coupling light into a waveguide is scattering, specifically by fluorescent molecules. The next chapter goes into the details of this subject of fluorescence and dipole radiation near interfaces. We will see that fluorescence is an important topic for a wide range of sensor applications.

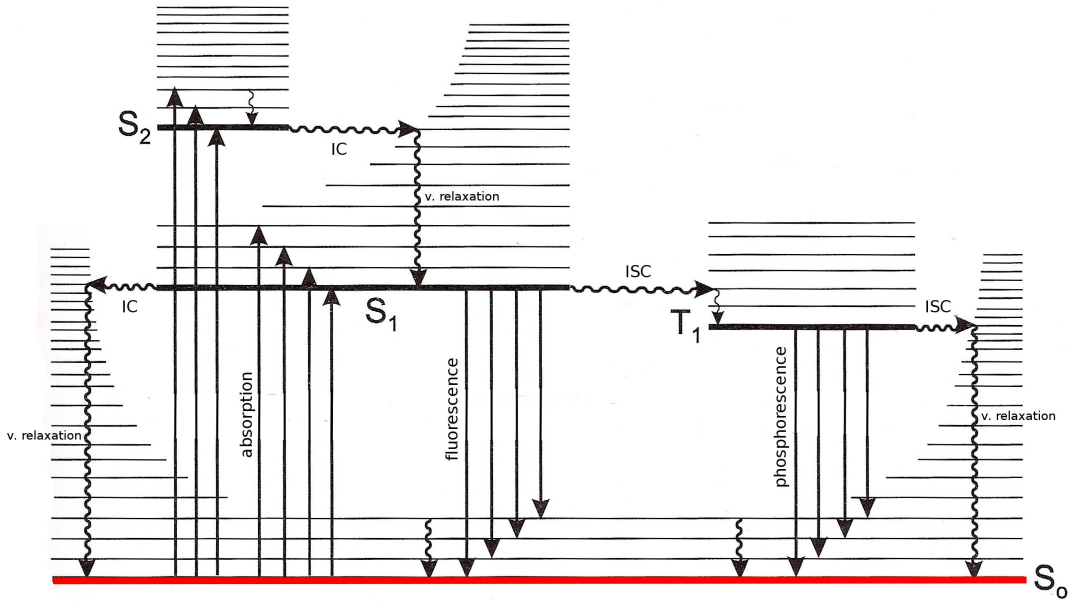

Figure 2.14: The Perrin-Jablonski diagram summarizes the possible excitation and de-excitation paths. Competing with fluorescence and phosphorescence are intersystem crossing (ISC) and internal conversion (IC).

2.2.2 Fluorescent molecules

Perrin-Jablonski diagram

To illustrate the main processes connected with fluorescence it is useful to show the Perrin-Jablonski diagram for a molecule. Boltzmann's law (Eq. (2.60)) gives us the fraction of molecules which are in an excited state N_1 with the energy E_1 at each temperature T, where k is the Boltzmann constant and N_0 the number of molecule in the S_0 state. At room temperature most of the molecules are in the lowest vibrational state of the fundamental singlett state S_0.

$$\frac{N_1}{N_0} = \exp[-\frac{E_1 - E_0}{kT}] \tag{2.60}$$

Starting at S_0, the absorption of a photon excites the molecule to any higher state, e.g. S_1 or S_2. Absorption is the fastest of all involved processes and takes place within 10^{-15}s. Depending on the excitation engery, it is also possible that the molecule ends up in a higher vibrational states. After exctiation, several radiative and non-radiative transitions, which lead to the energetic return of the molecule to the S_0 state, are possible.

Vibrational relaxation

Vibrational relaxation of an excited electron to the groud state of an electronic excitation takes place within around 10^{-12} to 10^{-10}s. Energy is thereby lost non-radiatively via collisions with the surrounding medium.

Internal conversion

Between two systems with the same spin state (e.g. S_2 and S_1) a non-radiative transition is possible if the two bands overlap each other. This internal conversion can also happen between S_1 and S_0 where, however, the probability is much lower.

Intersystem crossing

Intersystem crossing is connected with a change of spin state. Similar to internal conversion the molecules cross from the lowest vibrational singlet state S_1 to the first triplet state T_1. In general, the transition is "forbidden", strong spin-orbit interactions allow it to happen.

Fluorescence

Fluorescence is a radiative transition from the lowest vibrational S_1-state ro any vibrational state within S_0. The vibrational relaxation leads to the wavelength difference (called Stokes shift), which can be observed between the absorption and the emission spectra. The lifetime in the S_1-state before dropping down to the ground state is in the order of 10^{-10} to 10^{-7}s. Either inverted intersystem crossing from T_1 to S_1 or an interaction between two molecules in the T_1-state where one of them is transfered back to S_1 can also be followed by a deexcitation process to S_0. These processes are known as delayed fluorescence.

Phosphorescence

The equivalent deexcitation process from the T_1 state is phosphorescence. Apart from the fact that the molecule can stay longer (in the order of 10^{-6}s to a few minutes) in the first triplet state, it has to be noticed that the emission wavelengths are higher compared

to fluorescence. This follows from the fact that the energy level of the T_1-state lies below the one of the S_1-state.

Lifetime and quantum yield

To characterize radiation processes concerning fluorescence the lifetime of the S_1-state and the quantum yield are important quantities. As just discussed radiative and non-radiative processes starting from S_1 can occur. The only radiative process is fluorescence while on the other hand intersystem crossing and internal conversion happen radiationless. Here, vibrational relaxation to the lowest vibrational niveau is included in those two processes. The number of molecules in the excited state decreases according to Eq. (2.61) as a function of the sum of the radiative and non-radiative rates, k_r^S and k_{nr}^S.

$$C = C_0 \exp[-\frac{t}{\tau_S}] \tag{2.61}$$

$$\tau_S = \frac{1}{k_r^S + k_{nr}^S} \tag{2.62}$$

The quantity τ_S is the lifetime of the S_1-state. As the quantum yield of fluorescence is the fraction of radiative to total deexcitations it can be calculated by

$$y = \frac{k_r}{k_r^S + k_{nr}^S} = k_r \tau_S \tag{2.63}$$

Quenching

The prescence of gases, e.g. oxygen quenches fluorescence as it influences the quantum yield. Oxygen quenching takes place by molecular collisions and is more efficient if the S_1-state has a long lifetime. At higher temperatures collisions take place more often, the quantum yield is hence decreased. For phosphorescent materials (very long lifetimes) it is useful to cool the molecules to reach an increase of quantum yield. In sensor physics, apart from the prescence of oxygen and the dependence on temperature other quantities such as pH-value or polarity of the medium in which the molecules are embedded influence the quantum-yield of the molecules.

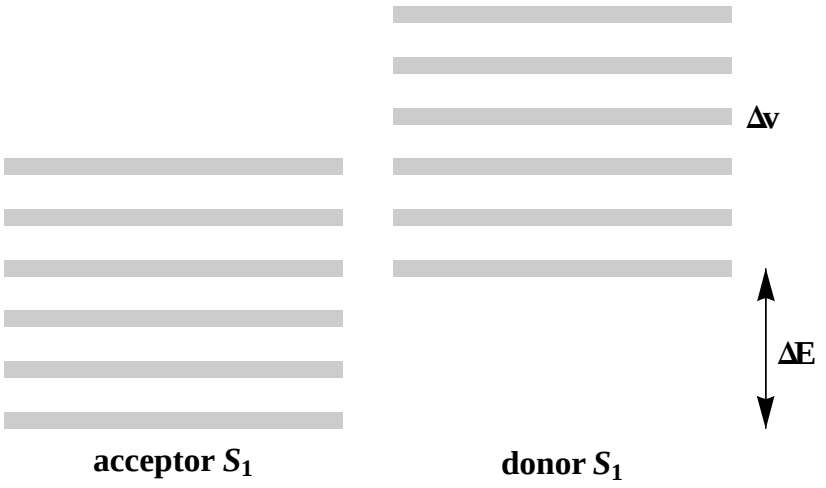

Figure 2.15: The non-radiative resonance energy transfer relies on an energy shift ΔE between the donor and the acceptor S_1-state. The vibrational states should still overlap each other so that they are in resonance with each other.

Energy transfer

In a two component system the excitation energy transfer from one molecule to another can happen radiatively as well as non-radiatively. In both cases the emission spectrum of the donor needs to overlap the absorption spectrum of the acceptor to make energy transfer possible. Energy transfer can be, e.g., used to widen the Stokes shift in a two-molecule system (compare Ch. 4). In the radiative case the emitted photon of molecule A (donor) excites the molecule B (acceptor). This process is important at distances larger than the wavelength of light.

The non-radiative process, which is known as resonance energy transfer (RET), gets important at lower distances. Other than for radiative transfer, the quantum yield of the donor influences the energy transfer. The term resonance results from the fact that vibrational S_1-states of the acceptor are, compared to the donor S_1-state, shifted by an energy ΔE in a way that each of the niveaus still has the same energy as one of the donor vibrational states. Let us assume that ΔE is three times the energy distance between nearby vibrational levels. An acceptor-excitation from the lowest vibrational state of S_0 to the fourth vibrational state of S_1 couples (or is in resonance) with a donor deexcitation from the lowest vibrational state of S_1 to the fourth vibrational state of S_1.

Three different interaction cases have to be distinguished. Depending on the strength of the molecular interaction energy U in relation to ΔE, the absorption bandwidth Δa and the bandwidth of the vibrational states Δv, they are classified into strong, weak and very weak coupling. In the case of strong coupling coulombic interaction play the most

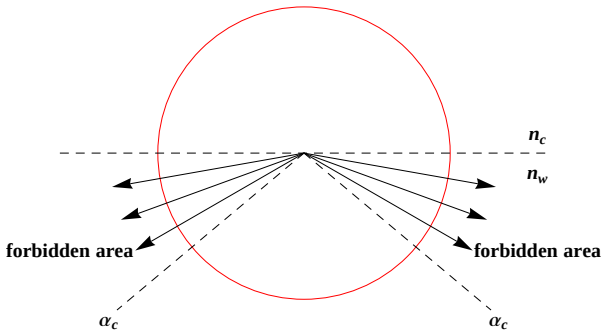

Figure 2.16: A dipole near an interface can radiate into different areas. The classically "forbidden" area beyond the critical angle is accessible from the electromagnetic viewpoint including evanscent waves. The refractive index of the upper halfspace (n_C) is lower than the one of the lower halfspace (n_W).

important role, while for very weak interaction dipole-dipole interaction is dominant.

- strong interaction: $U \gg \Delta E$, $U \gg \Delta a$, $U \gg \Delta v$
- weak interaction: $U \gg \Delta E$, $\Delta a \gg U \gg \Delta v$
- very weak interaction: $U \ll \Delta v \ll \Delta a$

For very weak coupling Theodor Förster derived an equation for the energy transfer rate constant k_{DD} in dependence on the distance between the donor and the acceptor. The Förster radius R_0 is the distance at which the spontaneous decay rate constant k_D and the energy transfer rate constant are equal and is typically below 10nm. [16, 17, 18]

$$k_{DD} = k_D(\frac{R_0}{r})^6 \tag{2.64}$$

2.2.3 Dipole radiation near an interface

Fluorescent molecules are dipoles, which change their radiation characteristics if they are brought close to interfaces. For a dipole above a waveguide there are different areas where radiation power can emerge. From the geometric optical viewpoint besides the upper half P_{up}, light can also reach an "allowed area" in the lower halfspace with an angle below the critical angle P_a. Expanding to the electromagnetic viewpoint the intrinsic evanscent field of the dipole can also reach an area P_f, which would be classically "forbidden".

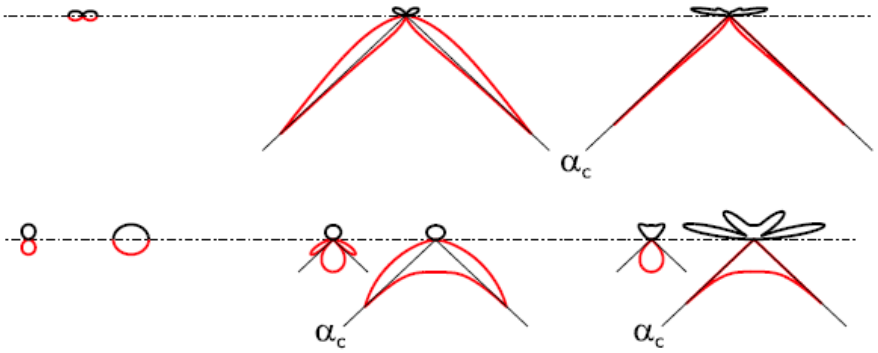

Figure 2.17: Comparison of the radiation characteristics for two dipole orientations, with the dipole axis located perpendicular and parallel to the surface (three different dipole distances relative to the interface each). The left side shows the radiation characteristics for a dipole at distance much larger than the wavelenght of light. In the center the dipole touches the interface, while on the right side the dipole is located at a distance of one wavelength. [16]

Different dipole orientations

At distances from an interface much larger than the wavelength of light the radiation characteristics of a dipole is the same as in a homogenous medium. It shows the typical donut-shape and has a cross-section looking similar to the ∞ symbol. As the dipole gets closer to the interface the radiation characteristic changes. At a distances smaller than roughly one wavelength the upward radiation is flattened while the largest part of the light is radiated into the direction of the critical angle. When the dipole is in contact with the interface a non-neglectable part reaches the "forbidden" area beyond the critical angle (compare Fig. 2.17). It is also important that the total radiation power of a dipole near an interface is larger compared to the free dipole, which can be explained by a lower fluorescence lifetime. In Fig. 2.17 the differences between two dipole orientations are illustrated. [7, 19]

2.2.4 Out-coupling

In the experimental section two different outcoupling mechanisms are investigated. Similar to end-fire coupling the end face of the waveguide couples a part of the light out. In fact, the outcoupling should be lower if the surfaces are rough (e.g. after cutting the waveguide). A second approach is to use scattering molecules placed on top of the waveguide core, which have the advantage that, due to the redirection of the light, the condition of the end faces does not influence out-coupling. The redirection makes it

possible to construct integrated sensor devices (compare Fig. 1.1) and allows detection by a photodiode.

Chapter 3

Simulation

In this chapter simulations on the propagation of light inside a waveguide are presented. Apart from the evaluation of the transcendental equation (2.42) with MATHEMATICA, applied to calculate the profile of modes inside an asymmetric waveguide, the software ZEMAX was used to do ray tracing simulations.

3.1 Numerical analysis of the transcendental equation

As a continuation of the theoretical treatment in the preceding chapter the goal of this section is the analysis of the transcendental equation 2.42. The solution is similar to the one presented in [11]. With MATHEMATICA the left part ($tan(h\kappa_w)$, blue curve in Fig. 3.1) and the right part ($\frac{\gamma_c+\gamma_s}{\kappa_w[1-\frac{\gamma_c\gamma_s}{\kappa_w^2}]}$, red curve in Fig. 3.1) of Eq. (2.42) were plotted over κ. The refractive indices were set to $n_w = 1.59$ (waveguide), $n_s = 1.42$ (substrate) and $n_c = 1.00$ (upper cladding, air) similar to the materials polystyrene and PDMS, which will be used in the experimental section. As it was chosen to do the calculations in the unit μm the thickness of the waveguide was set to 10 μm and the wavelength (according to the emission peak of the resonance energy transfer system in the experimental section) to 0.650 μm.

To achieve the numerical solution of the transcendental equation a starting search value $\kappa_{min} = 0.2$ was defined. With a search stepsize of $\Delta\kappa = 0.1$, 22 different values for κ were obtained allowing to calculate the corresponding values for β, γ_s and γ_c.

All of those parameters were now introduced into the three solutions of the transcendental equation (see Eq. (2.39) - (2.41)) to be able to plot the solution inside and outside of the waveguide. In Fig. 3.2 and Fig. 3.3 the solutions for m = 0 - 8, 11, 12, 19 are presented by plotting the intensity of the electrical field $E_y(x)$ (pointing in the y-direction, analog to Sec. 2.1.2) over the position x [μm] in the waveguide. The ordinate defines the interface boundary air/polystyrene while the dashed line indicates the polystyrene/PDMS

Table 3.1: Longitudinal and transversal components for modes of order m in a 10 μm waveguide.

m	κ $[\mu m^{-1}]$	β $[\mu m^{-1}]$	m	κ $[\mu m^{-1}]$	β $[\mu m^{-1}]$	m	κ $[\mu m^{-1}]$	β $[\mu m^{-1}]$
0	0.307145	15.3666	8	2.76299	15.1192	16	5.21025	14.4596
1	0.61428	15.3574	9	3.06962	15.06	17	5.51458	14.3463
2	0.921394	15.342	10	3.3761	14.9943	18	5.81818	14.2258
3	1.22848	15.3205	11	3.68242	14.922	19	6.12072	14.0983
4	1.53552	15.2927	12	3.98856	14.8431	20	6.42153	13.9639
5	1.8425	15.2588	13	4.2944	14.7575	21	6.71859	13.8234
6	2.14942	15.2186	14	4.60009	14.6651			
7	2.45626	15.1721	15	4.90538	14.5658			

interface. Note that the unit of the ordinate is arbitrary as the constant A in the Eqs. (2.39) - (2.41) was disregarded. It can be clearly seen that, as mentioned before, higher order modes reach further into the cladding even though their amplitude gets smaller with increasing mode number. The figures also point out that evanescent waves decay faster if the refractive index difference at the interface is higher (at the right interface $\Delta n = 0.59$, while at the left interface $\Delta n = 0.17$). The mode number is as expected equivalent to the number of nodes of the mode.

3.2 Ray tracing

While in computer graphics ray tracing is used for image generation, in physics it is used to model the propagation of light through optical systems. By introducing rays it is possible to calulate the path of particles or waves, which propagate inside a material with certain optical properties. In general ray tracing is based on geometrical optics following Snell's law together with propagation velocity differences. Anyhow, other electromagnical properties, e.g. polarization, wavelength or diffraction, can also be taken into account by the implementation of appropriate physical principles (as, e.g., the Fresnel equations). Rays are normal to the local wavefront, point into the direction of the energy flow and include information such as direction, position, phase and amplitude. An important assumption is that those rays are - within a small section - straight. When a ray passes from one section to the other, ray tracing is done by adapting the properties of the ray at each interface. Basically the preset attributes of rays have to fit the given task to achieve correct solutions. If the spatial dimension of the simulated system is large compared to the wavelength, by using a large number of rays real optical systems can be simulated precisely. Optical design progams often make use of ray tracing simulation.

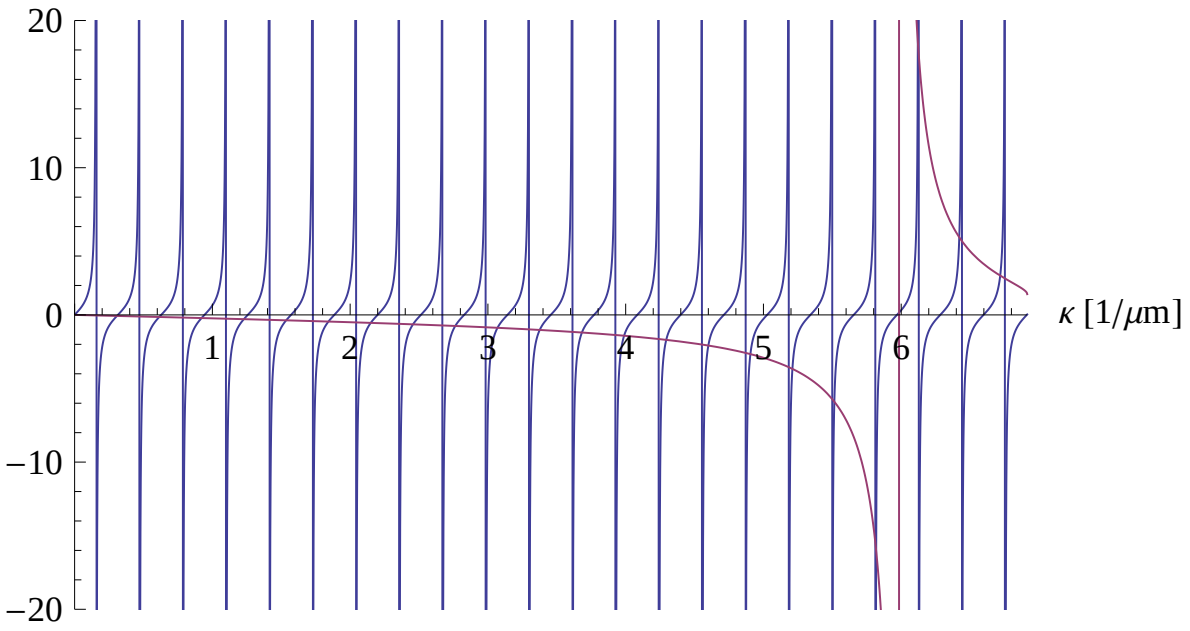

Figure 3.1: Plot of the left hand side (blue lines) and the right hand side (red lines) of the transcendental equation Eq. (2.42). The ordinate illustrates the function value of each side of the transcendental equation in arbitrary units

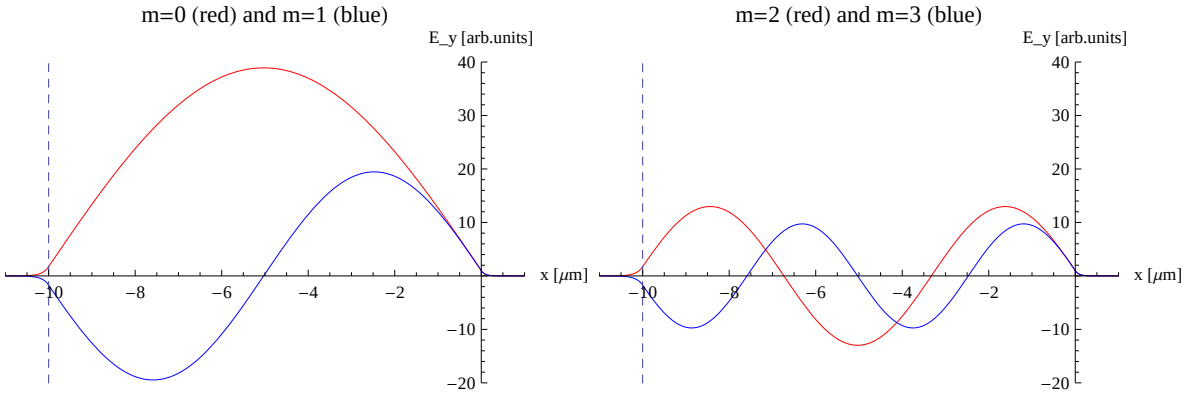

Figure 3.2: Comparison of the transverse electric modes m=0,1,2,3 of a 10 μm waveguide. The polystyrene core is surrounded by air (right side of the E_y axis) and PDMS (left side of the dashed line).

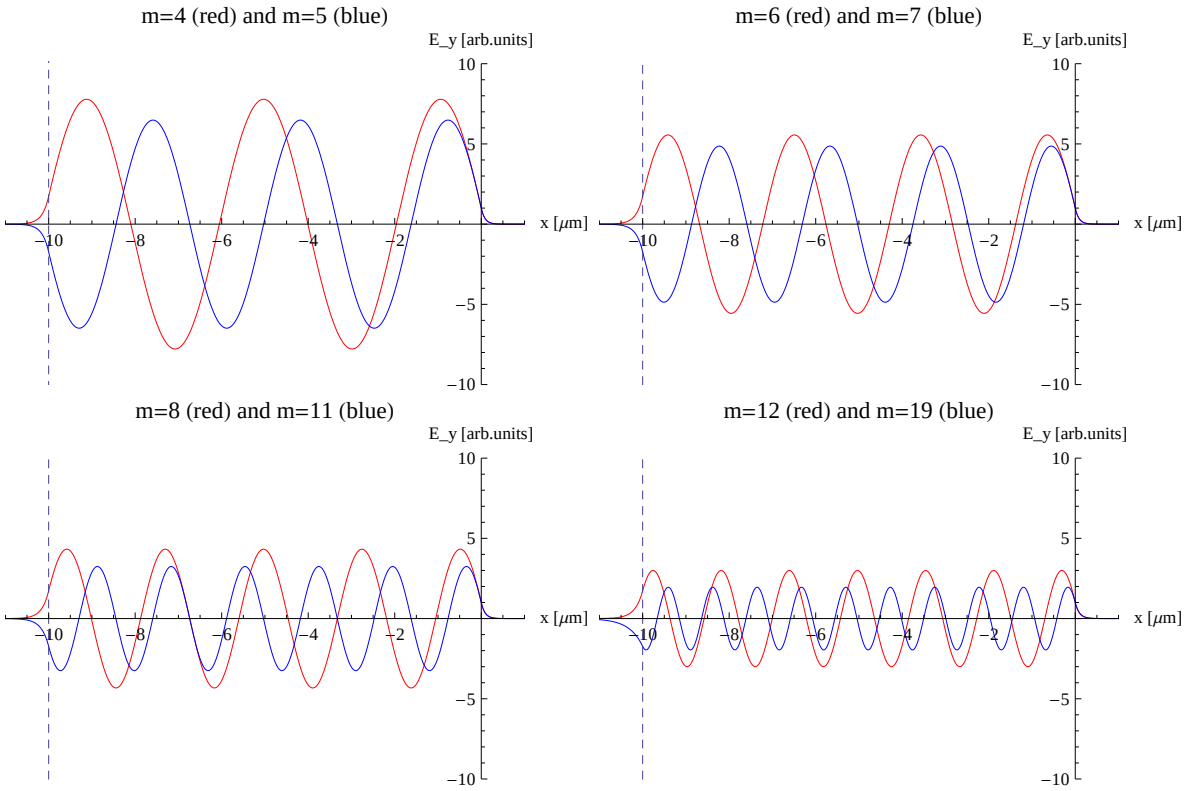

Figure 3.3: Profile of the transverse electric modes m=4,5,6,7,8,11,12,19 of a 10 μm waveguide. The polystyrene core is surrounded by air (right side of the E_y axis) and PDMS (left side of the dashed line).

In this chapter the software ZEMAX by the ZEMAX Development Corporation was used. Depending on the application, ZEMAX can operate in two different modes, sequential and non-sequential. Sequential means that all optical paths are followed in a strict order. Light can therefore not pass from one interface to a second and then back to the first. This method is useful for simulating lenses, microscopes or telescopes. A second way is non-sequential ray tracing, which has to be favored for waveguide simulation and allows multiple interactions of one ray with a surface. Combining geometrical optics with wave optics, Zemax uses an approximation method called "Physical Optics Propagation" (POP), which considers diffraction phenomena as well. In this method each ray is given by an array of points, with each point having a certain complex amplitude corresponding to its electric field. The phase of this complex number gives us the phase of the wavefront, the amplitude corresponds to the power of the beam. For the propagation of the wave an algorithm is used, which relies either on Fresnel diffraction or on the angular spectrum method [20]. At each surface a transfer function is calculated which changes the ray parameters. [21]

3.2.1 Description of the simulated system

In the experimental section fluorescent molecules will be included inside a polystyrene core material on top of a PDMS cladding. As a comparison, the propagation of light, which is emitted from a point source is investigated in this section. For all simulations a point source is located in the center (compare Fig. 3.4 and 3.5) of a rectangular volume with a refractive index of n_w=1.59 (polystyrene), which is placed on top of a low-refractive index volume (n_c=1.42, PDMS) with the same length and width. The lower side of the cladding is assumed absorbing and the whole system is surrounded by air (n_s=1.00). The intensity arriving at different rectangular detectors planes was simulated and between 1 and 10 million rays were traced. The height of the cladding material was in all cases chosen to be 10 mm, its thickness should however not influence the simulations because the lower side of the cladding is absorbing. A general overview of the system is shown in Fig. 3.4, the location of the point source can be seen in Fig. 3.5. For all of the following simulations splitting and scattering of rays was allowed and the source wavelength was chosen to be 0.650 μm. Furthermore, a point source in ZEMAX is randomly polarized leading to the fact that on interaction with an interface s and p polarization is averaged.

Rays can be detected by detector objects, which are able to display angular and spatial data of light that lands upon them. A rectangular detector is a two-dimensional array of pixels (comparable to a CCD-array). The total detected intensity data can be displayed in photometric units such as watts, lumens or lux, while the intensity of each pixel is normalized to $\frac{watts}{cm^2}$ respectively. The scale for the pixel intensities is displayed by a bar on the right side of the detector image, and can be chosen to be, e.g., in false color or gray scale. A detector can constist of air (which means that the rays pass through the

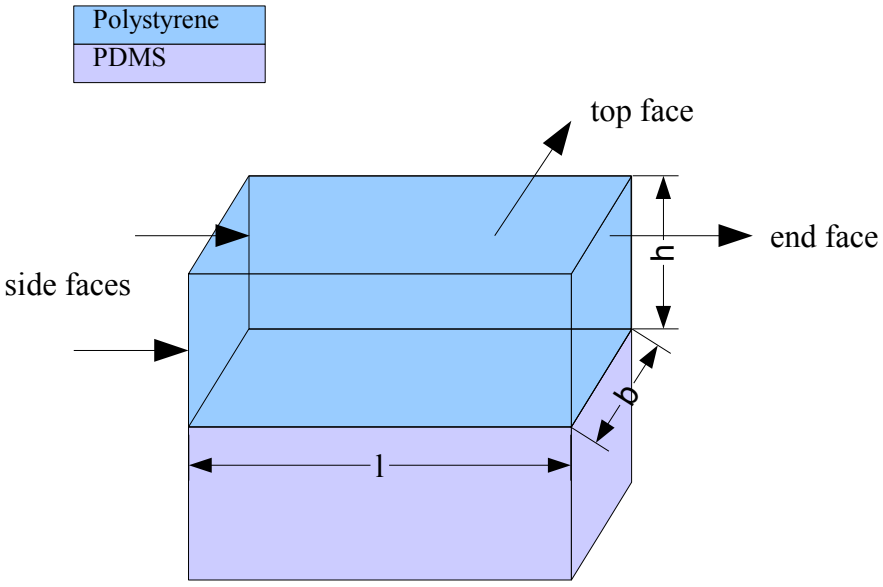

Figure 3.4: Sketch of the system used for ray tracing simulation with ZEMAX. Two rectangular volumes with different refractive indices (PDMS n=1.42 and polystyrene n=1.59) were placed on top of each other.

detector without being perturbed), furthermore it can also be absorbing or a mirror. In a database file more information of each ray, e.g., the intensity, the polarization, the path length or the direction cosines, can be stored and analyzed.

3.2.2 Comparison of different absorbing conditions

In this section two different absorbing conditions for the waveguide faces are compared to each other and estimation for the throughput of the system is done. Either all of the waveguide faces (side faces, front face, end face) are absorbing or just the end face is non-absorbing. The label "all faces absorbing" of course excludes the lower and top face of the waveguide, which makes waveguiding possible. In this simulation the waveguide has the dimensions l=60 mm, b=30 mm and h=10 mm. In the middle of the core material at the position l_0=1 mm a point emitter radiates with a total intensity of 1 W and a wavelength of 650 nm isotropically in all directions. The position of a rectangular detector inside the waveguide, which has the same size as the end face, was varied (compare Fig. 3.5). For the calculation of the spatial throughput at each

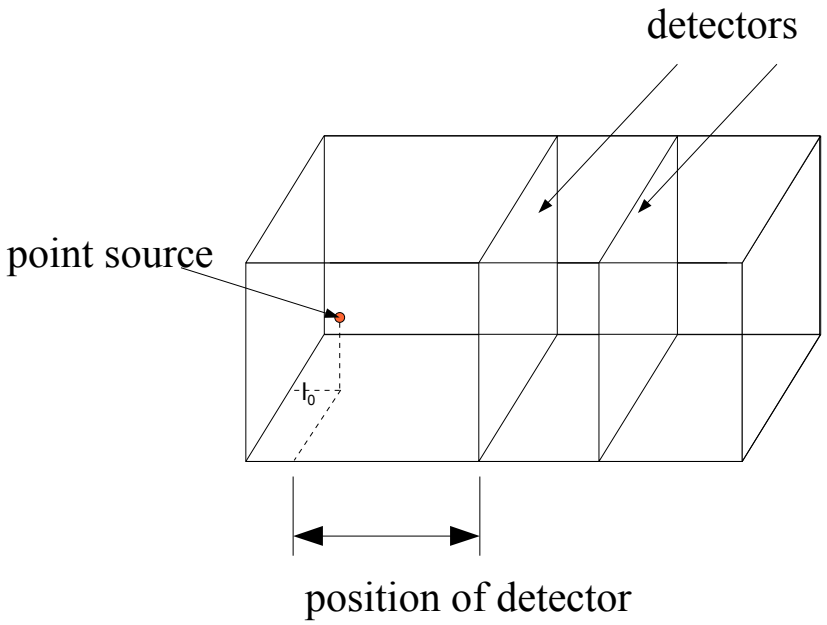

Figure 3.5: In the center of the polystyrene layer a point source radiates isotropically. The guided intensity is detected by rectangular detecors of the same size and parallel to the end-face.

distance Eq. (4.1) was used with $I_{edge} = I_{detector}$, corresponding to the total intensity on the detector, and $I_{LED} = I_{pointsource} = 1W$, corresponding to the intensity of the point source. This leads to the equation $TP\,[\%] = 100\frac{\pi}{\arctan\frac{b}{2l}}\frac{1}{I_{detector}}$, where l is the distance of the rectangular detector to the point source in z-direction and b the width of the waveguide. In general the throughput gives us in this case the intensity in a total of 360° relative to the point source. As the detectors are rectangular this is only an approximation to compare the total intensity inside a waveguide at different distances to the point source. It also was done to give comparable results to the experimental section. For more information on the throughput see Sec. 4.3.2.

As shown in Fig. 3.6 the throughput measurements in an asymmetric waveguide ("all faces absorbing" and "end face not absorbing") are roughly equal and tend to a constant throughput of around 47%. The increase close to the end of waveguide (Fig. 3.7), in the case in which the end face is not absorbing, can be explained by the fact that part of the light emerging from the waveguide at the end face will be reflected back due to Fresnel reflection and is thus detected twice at the dectector. In both cases at a length of around 30 mm the throughput stays constant and as all of the light is guided in the waveguide an equilibrium is reached. For comparison the same simulation was done for a symmetric polystyrene/air waveguide without cladding. Due to the higher angle of total reflection the equilibrium is reached much earlier (at around 5 mm) and the throughput approaches 78%. This simulation tells us that the condition of the end face

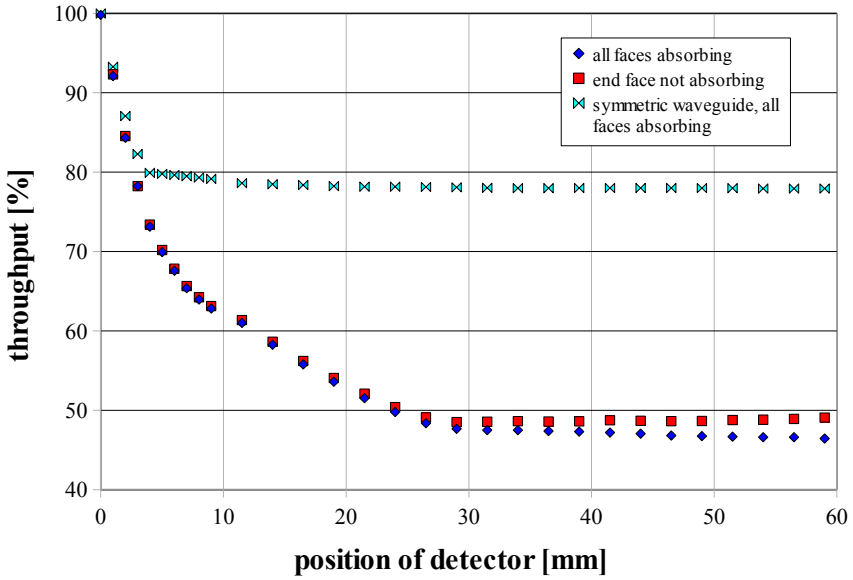

Figure 3.6: Comparison of the throughput in dependence of the detector position. Two different absorbing conditions are compared to a symmetric waveguide.

does not influence the measured signal to a great extent. It gives an estimation for the theoretical maximum throughput in an asymmetrical waveguide with a core refractive index of n_w=1.59, surrounded by two claddings with n_c=1.42 and n_s=1.00. This result has to be compared with the experimental results in Sec. 4.3 .

3.2.3 Throughput for different core heights

In Fig. 3.8 simulations as in Sec. 3.2.2 were done for two different core heights, h=10 mm and h=4 mm. The heights are chosen to be a larger than in the experimental section (10 - 17 μm) to reduce the simulation duration, which is dependent on the number of interactions with interfaces. The system dimensions were again chosen to be l=60 mm and b=30 mm and all the faces of the waveguide were set to be absorbing. In the thinner case the equilibrium is reached much faster than for the thicker waveguide due to the fact that rays below the critical angle reach the interface earlier and therefore have the chance to leave the waveguide at a shorter distance. Both measurements tend to a comparable throughput value of about 47%, which lets us assume that the throughput is in this case independent on the thickness of the waveguide. In the experimental part the electromagnetic viewpoint will be discussed as a comparison to this result. The equilibrium will be reached at very short distances as the waveguide will have a thickness in the order of 10 μm.

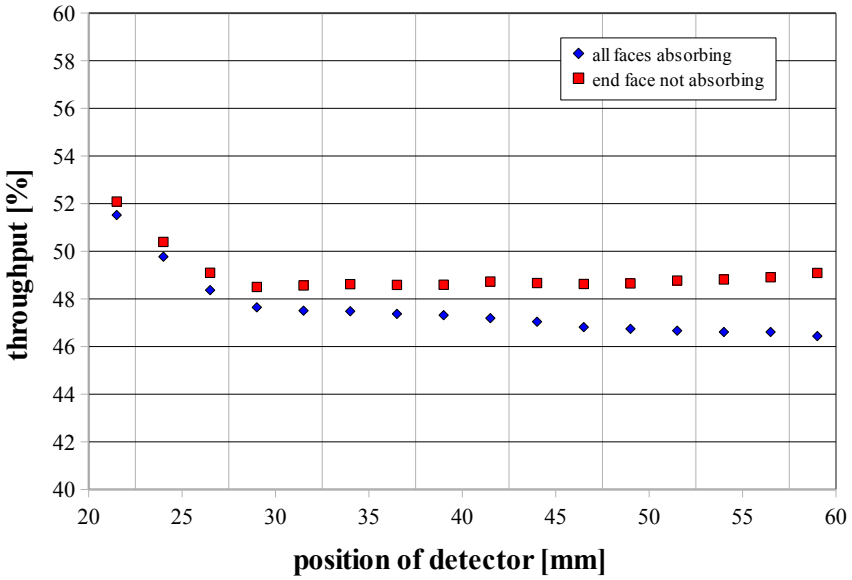

Figure 3.7: Magnification of Fig. 3.6. The increase of the throughput in the case in which the end face is non-absorbing results from partial reflection of the rays hitting the end face.

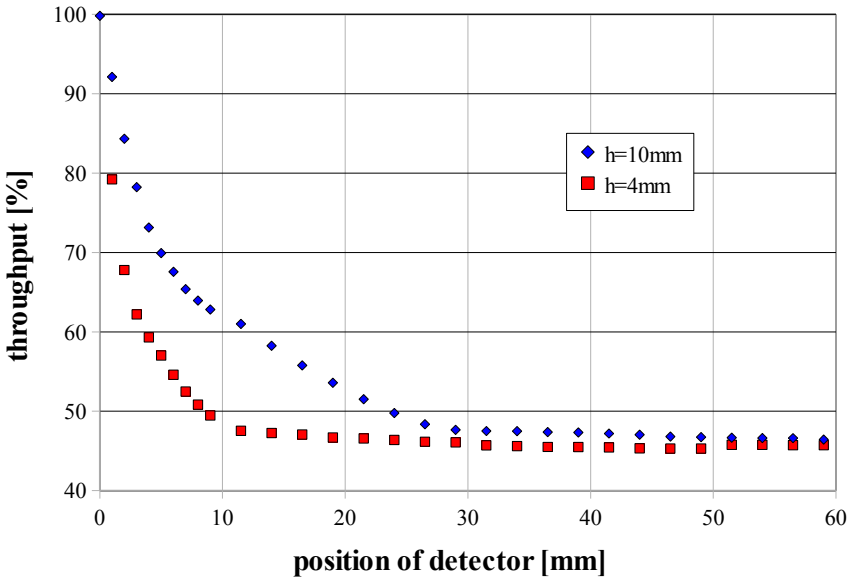

Figure 3.8: Throughput in dependence of the detector position for two different core thicknesses, h=10 mm and h=4 mm.

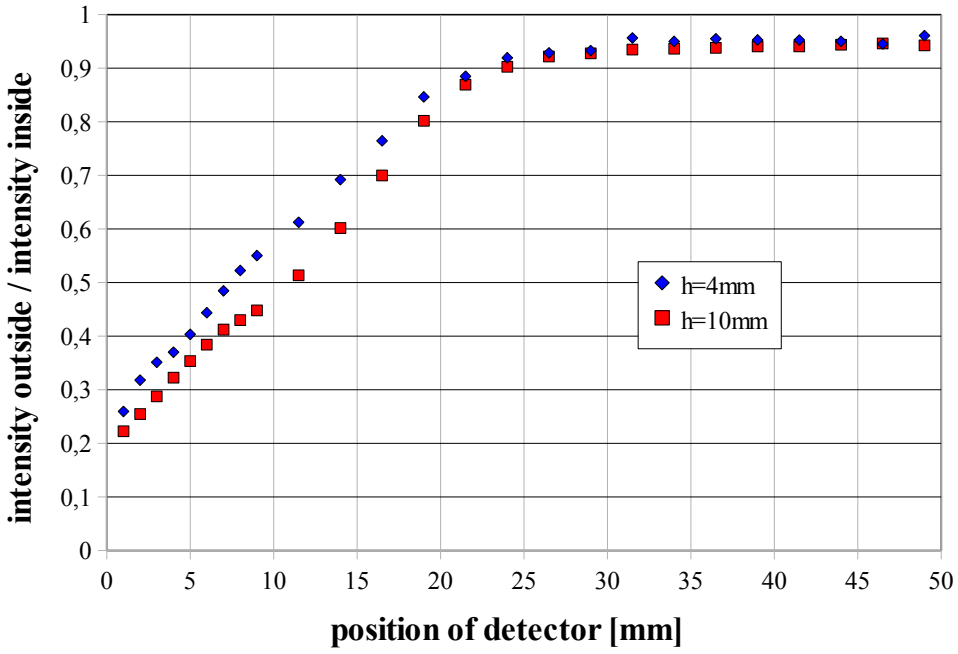

Figure 3.9: Relative out-coupled intensity (intensity outside/intensity inside) at different waveguide lengths. At lengths larger than 25 mm more than 90% of the signal is coupled out.

3.2.4 Out-coupling simulation

To calculate the amount of light which is coupled out in this waveguide configuration, the amount of light which travels inside the waveguide was simulated for a system with the same dimensions as before (l=60 mm, b=30 mm) for two different thicknesses h=10 mm and h=4 mm. Those intensities were then compared to the amount of light outside the waveguide, while the waveguide length was reduced. For that the detector was placed just outside (0.001 mm) the end face. It is important to notice that for the intensity measurement inside the waveguide the length was kept constant and all faces were absorbing. On the other hand for the measurements outside the waveguide, the length of the waveguide was reduced stepwise to be able to place the detector in the surrounding material close to the end face. To reach comparable results all detectors had the same size as the end face.

Figure 3.9 shows the comparison (intensity outside/intensity inside) of the two measured signals over the position of the waveguide. At shorter distances only a small amount of light is coupled out. A bigger fraction of the rays which hit the end face have an angle below total reflection and are able to leave the waveguide. As an illustration, in Fig. 3.10 the thick red ray has the critical angle of total reflection. All rays with a bigger angle

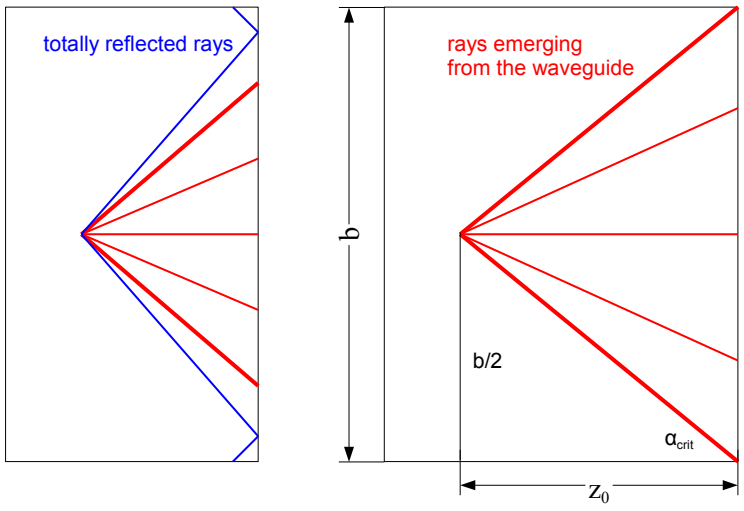

Figure 3.10: Top view of the waveguide. Depending on the length of the waveguide some of the light is able to emerge (red) while rays with an angle beyond the critical angle are reflected. Beyond a certain length z_0 all of the rays leave the waveguide, as shown on the right hand side.

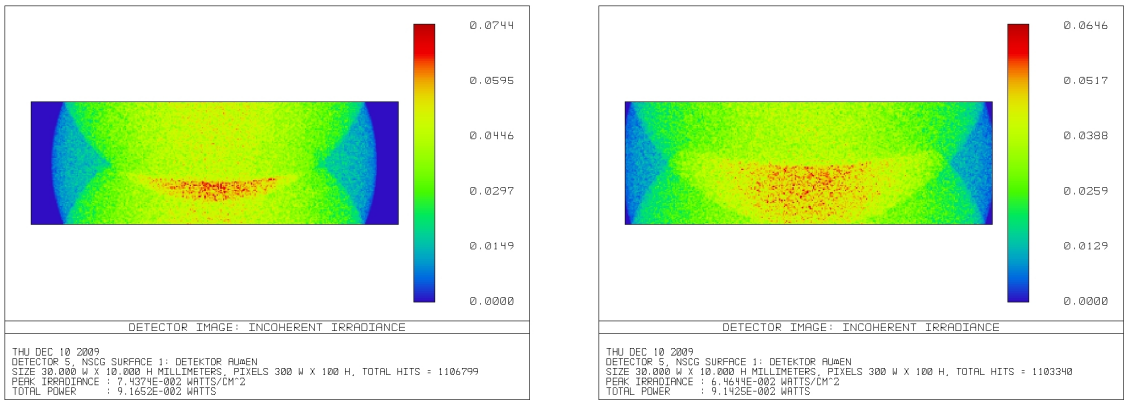

Figure 3.11: Comparison of two distributions for detectors placed just outside the waveguide. The rectangular detectors are placed 0.001mm outside the end face orthogonal to the z-direction. On the left side, at a detector position of 17.5 mm a part of the detector is still dark, as some of the light is totally reflected back. On the right hand side, at 20 mm, the whole detector is bright, because the critical distance z_0=18.5 mm was reached.

(colored in blue) will remain inside the waveguide because they are totally reflected. The longer the waveguide gets the lower the fraction of rays, that lie beyond the critical angle. At a certain critical distance z_0 all rays are able to emerge from the waveguide. Based on simple geometry z_0 can be calculated by $z_0 = \frac{b/2}{tan(\alpha_{crit})} = \frac{15}{tan(39°)} = 18.5$ mm as demonstrated on the right hand side of Fig. 3.10. Figure 3.11 shows two detector images outside the waveguide for 17.5 mm and 20 mm to demonstrate out-coupling. Blue color corresponds to low intensities, red color to high intensities, the special shape of the intensity distribution will be discussed in the following section. We can see that at 20 mm the whole detector is illuminated, while at a lower distance of 17.5 mm the outer part is still dark. This observation conforms with the calculated value of z_0=18.5 mm.

The reason why in Fig. 3.9 the constant value of around 93% is reached beyond 25 mm is expected to be due to the fact that even when leaving the waveguide a part of the ray is reflected according to the Fresnel coefficients. Theoretically the maximum out-coupled signal should approach 96% for a very long waveguide as even in the orthogonal incidence 4% is reflected back. The difference of around 3% results from the fact that the waveguide is not infinite. In the following experiments (compare Sec. 4.3) almost all of the light travelling inside the waveguide should be coupled out as we will use waveguides longer than 30 mm.

3.2.5 Equilibrium simulation

To find out how the propagation of light originating from a point source inside the waveguide takes place, the intensity arriving at rectangular detectors placed at different positions related to the point source was compared (see Fig. 3.5). Two cases were taken into account, either all faces were absorbing or just the side faces were non-absorbing. In the following figures red color belongs to a high and blue color to a low intensity. For detector positions below 10 mm the detector images in the absorbing and the non-absorbing case are equal. Exemplarily, in Fig. 3.13 the detector images (in the absorbing case) for detector positions from 3-10 mm are shown in false color. The distance between each of the detector images is 1 mm. At a detector distance of around seven millimeters rays which are totally reflected at the upper polystyrene/air interface begin to overlap (interfere) with the non refected rays as demonstrated in Fig. 3.12. The red ray travels at the critical angle of the polystyrene/air boundary. Furthermore, the same process takes place beginning at a distance of around 12.5 mm for the polystyrene/PDMS interface leading to further interference. The ray travelling at the second critical angle is highlighted in blue in Fig. 3.12. The figures 3.14 and 3.15 compare the two different cases with each other. On the left side all faces are absorbing, on the right side just the side faces are non absorbing. Differences begin to show at detector positions of about 12.5 mm when the rays hit the side faces. On the left side they are absorbed, while on the right side the reflections lead to interferences similar to those

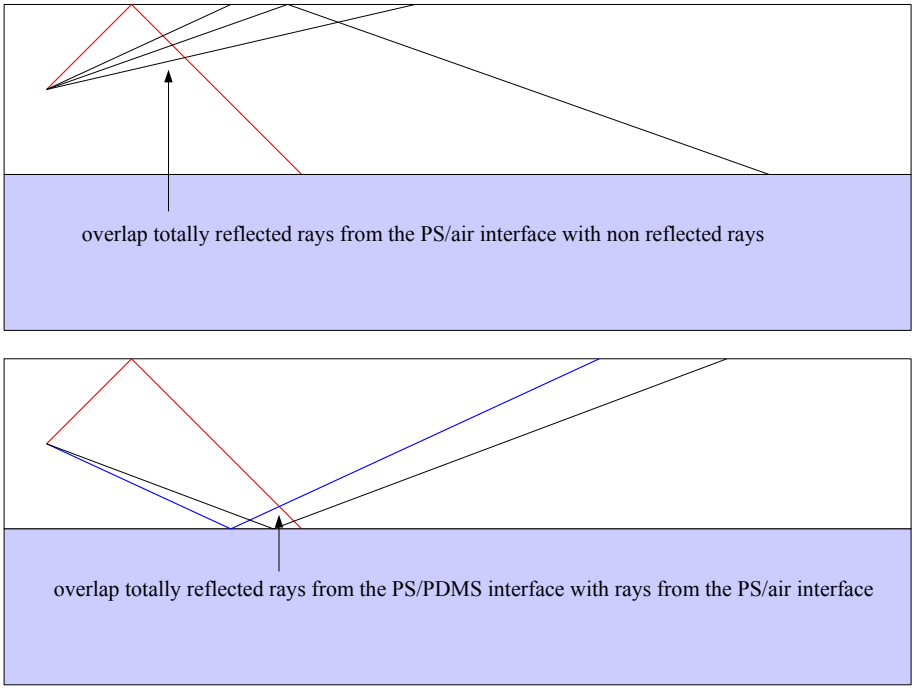

Figure 3.12: The upper picture sketch a ray (colored in red) travelling at the critical angle of the polystyrene/air interface which overlaps with the non reflected rays, leading to interference patterns at the detector. In the lower picture the same process takes place at the interface polystyrene/PDMS.

observed in Fig. 3.12. It also can be clearly seen that if the side faces are non-absorbing, the total intensity on the detector is higher. For the following experimental part we conclude that, if a point source is located in a waveguide, the intensity distribution will not be uniform, especially at lower waveguide lengths. Anyhow we have to be careful to draw practical conclusions about the side faces and end faces as they will be (due to the fabrication process of spin coating) not as smooth as the top and bottom face of the waveguide.

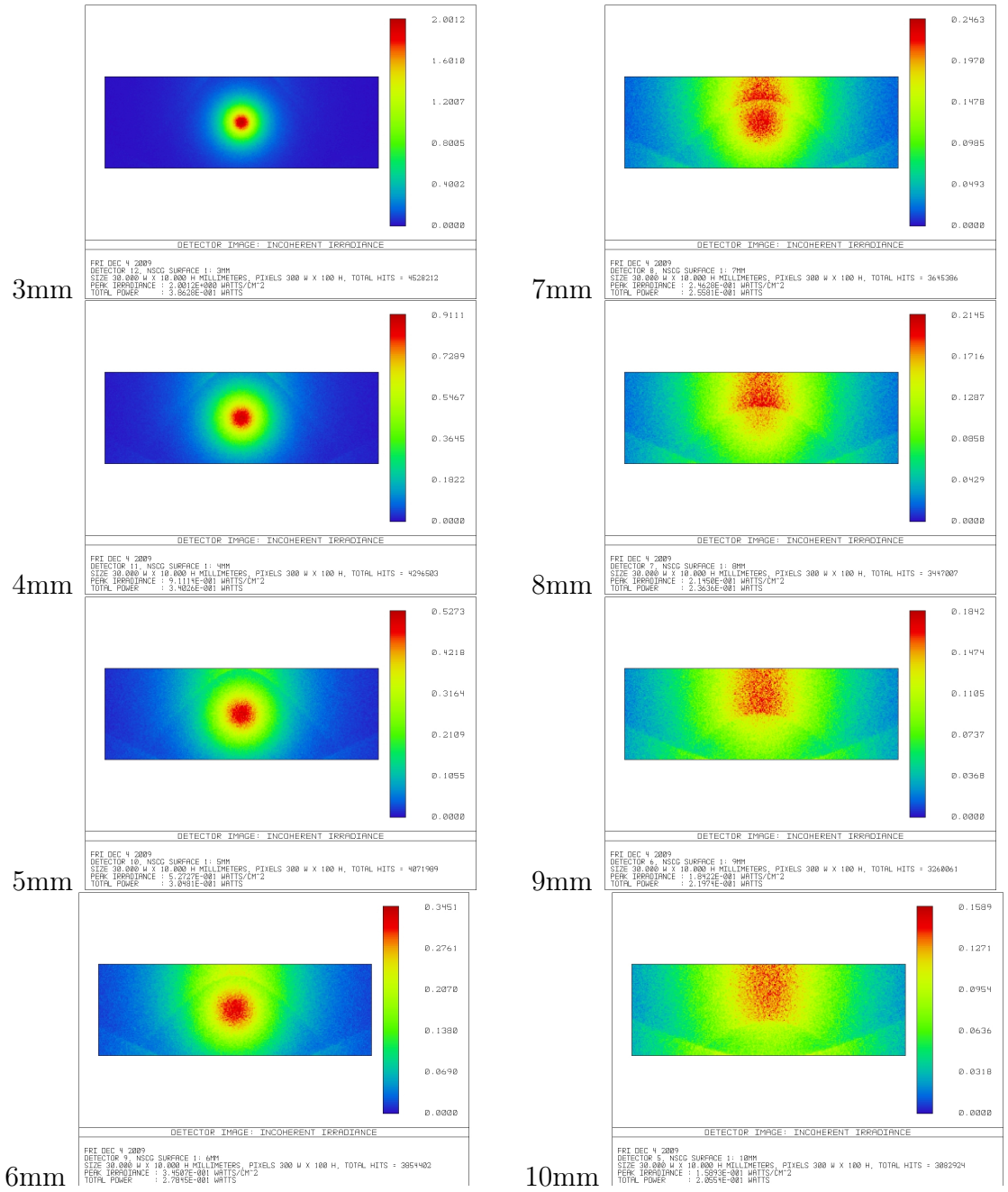

Figure 3.13: Intensities arriving on a rectangular detector inside a waveguide at detector postitions 3 to 10 mm away from the point source for the case were all faces are absorbing.

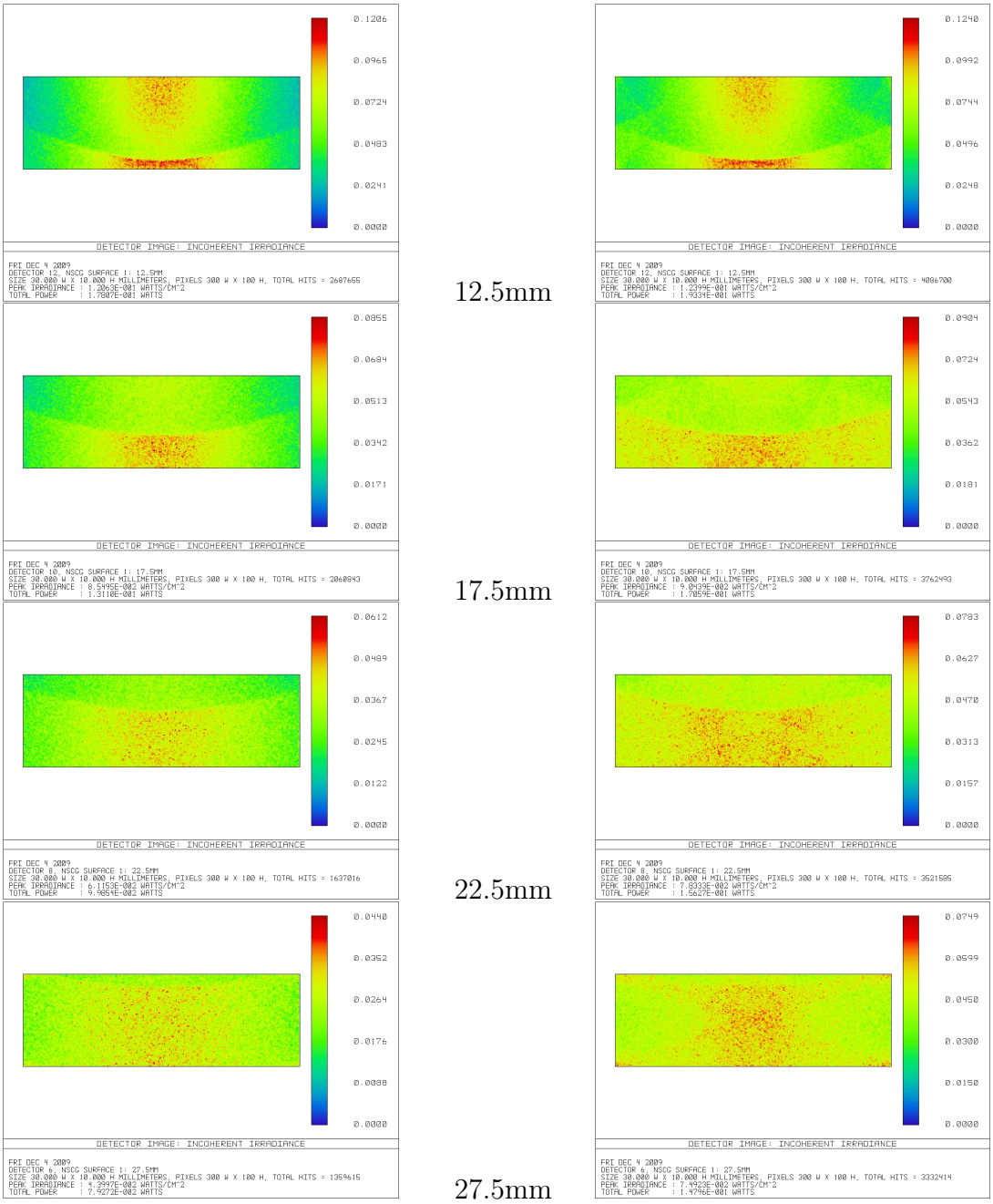

Figure 3.14: Intensities arriving on a rectangular detector inside a waveguide at detector postitions 12.5 mm, 17.5 mm, 22.5 mm and 27.5 mm away from the point source. The left side shows a waveguide, where all faces are absorbing, the right side a waveguide, where the side faces are non absorbing.

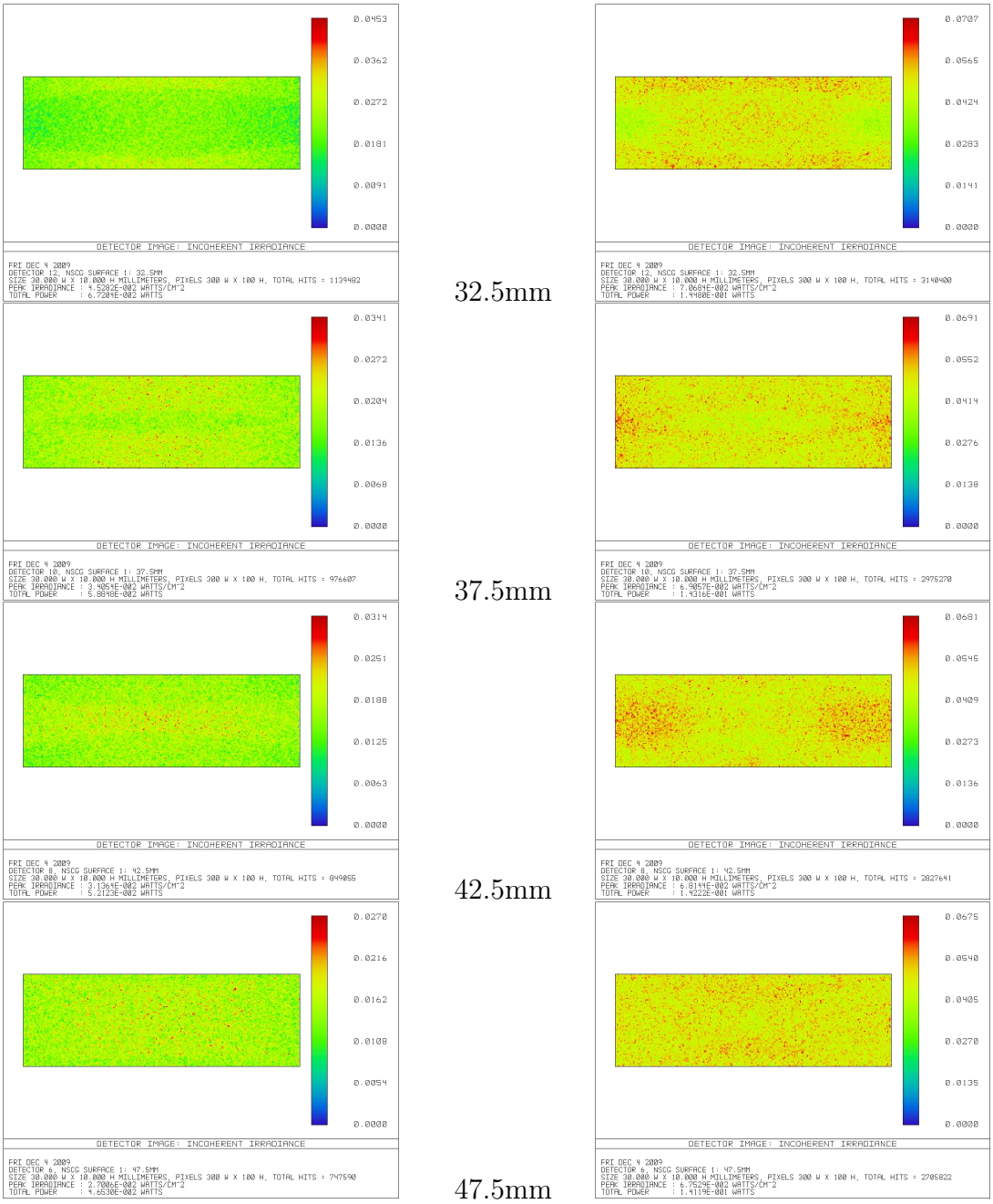

Figure 3.15: Intensities arriving on a rectangular detector inside a waveguide at detector postitions 32.5 mm, 37.5 mm, 42.5 mm and 47.5 mm away from the point source. The left side shows a waveguide, where all faces are absorbing, the right side a waveguide, where the side faces are non absorbing.

Chapter 4

Experimental

To be able to study different coupling mechanisms related to fluorescent molecules a basic sensor design has to be chosen. As mentioned before, a dielectric slab waveguide was used. The following chapter will describe the materials and methods used.

4.1 Materials

The question which materials to use is very important since there has to be a refractive index difference between the core and cladding. A large refractive index difference is favorable because it yields a larger amount of light (or a higher number of modes) travelling in the waveguide and thus makes detection easier. Preferably the whole sensor needs to be cheap and easy to fabricate. On the other hand for a future sensor application the core should be gas permeable while the Stokes shift of the fluorescent molecules has to be large to allow quenching-based applications and avoid reabsorption processes. Another topic is that as a lot of suitable core and cladding materials use similar solvents the interface boundary will not be well-defined in multi-step processes. Meeting all these requirements is a challenging task.

Figure 4.1 gives a basic overview of the planar waveguide used. A light emitting diode excites fluorescent molecules, which couple light into a planar waveguide. The cladding consists of polydimethylsiloxane with a polystyrene layer on top of it, which acts as the core of the waveguide. As the term ”throughput” will be used often in the following, it is useful to give an explanation in advance. The throughput is the intensity of light, that is detected after being coupled out of the waveguide, normalized to the excitation.

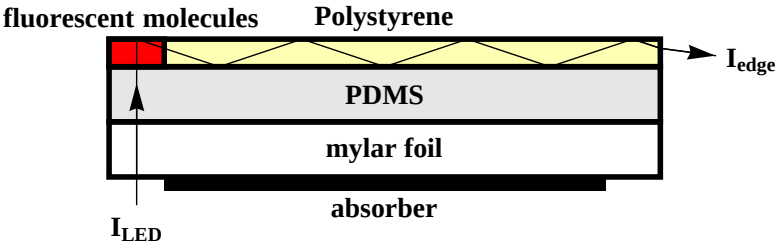

Figure 4.1: A basic sketch of the waveguide system.

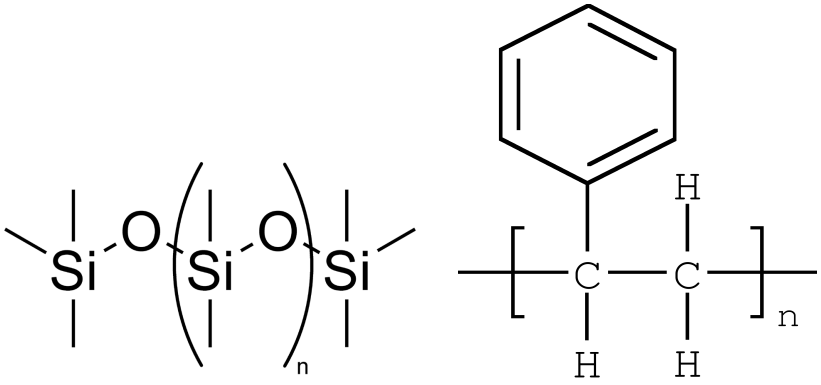

Figure 4.2: Molecular formulae of PDMS (left side) and polystyrene (right side).

4.1.1 Substrate

For selecting the "fundament" of the sensor, the substrate, flexibility is an important issue in organic electronics. The "Aluminum Oxide Lapping (Polishing) Sheet LFG5P" from Thorlabs consists of Mylar foil (polyethylene terephthalate) with a 5 μm absorbing silicon carbide layer on one side. The absorbing layer avoids the propagation of modes in the substrate. The total thickness of around 100 μm allows easy cutting and gives the requested flexibility.

4.1.2 Polydimethylsiloxane (cladding)

Polydimethylsiloxane (PDMS, compare Fig. 4.2) belongs to the group of the polysiloxanes. Polysiloxanes consist of silicon-oxygen chains of different length, which can form linear or cyclic geometries. At the remaining branches of the silicon, different groups can be attached, in the case of polydimethylsiloxane it is methyl. Depending on how many bondings to oxygen each silicon group has, they are named as mono (M), di (D), tri (T) or quattro (Q). Polydimethylsiloxane has in the center n groups with two oxygen bonds and two methyl-groups and at each end a silicon-atom with one oxygen bond

and three methyl-groups. It can therefore be abbreviated by MD_nM, which stands for $R_3SiO[R_2SiO]_nSiR_3$, where R here is CH_3. Polydimethylsiloxane is characterized by its high temperature (up to 250°C) and UV resistance, which can be explained by the strength of the $Si-O$ bonding. Furthermore, it also shows a high elasticity even at low temperatures, high resistance against oxidizing chemicals and high gas permeability compared to other polymeres. Due to its low surface energy, polydimethylsiloxane shows low adhesion to other materials. This fact can, for example, be countered by a low pressure O_2-plasma treatment, which leads to functional groups including oxygen at the surface but is accompanied by etching. [22, 23, 24]

The polydimethylsiloxane Sylgard 184, which was used in the experimental section, is a two component system and consists of a base and a curing agent which have to be mixed thoroughly with the ratio of 10:1. To remove air-bubbles from the mixture a vaccuum treatment was done. After mixing the two components it has to be used within two hours before it starts to harden. When the processing is finished, it is necessary to cure the material that it reaches its final cross-linking. The manufacturer suggests to choose between three cross-linking times and temperatures, 15 minutes at 150°C, 60 minutes at 100°C or 4 hours at 65°C. The main advantages of Sylgard 184 are its low refractive index of 1.43 (after 4 hours baking at 65°C), its flexibility and it resistance to solvents. It is therefore used as a cladding material. [25]

4.1.3 Polystyrene and ethylcellulose (core)

Polystyrene (compare Fig. 4.2) is a widely used plastic with fields of applications in, e.g., electronics or packaging. It consists of a chain of single bonded carbon atoms, where at every other carbon bonding a phenyl group (benzene) is added. The other free carbon bondings are occupied by hydrogen atoms. Its high refractive index of 1.59 and its permeability makes it an ideal waveguiding material for sensor applications. In the experimental section it is also used as a matrix material for the fluorescent molecules. Other advantages are the thermal stability and the low cost of the material. Polystyrene is solved in anisole to be able to spin coat it on the cladding layer. Alternative solvents would be toluene or benzene. An alternative waveguiding material, here used for resonance energy transfer (RET) measurements, would be ethylcellulose. It is solved in a mixture of toluene/ethanole, has a lower refractive index of 1.47 and also shows high permeability. The basic idea behind the usage of ethylcellulose as a matrix material was to improve light coupling by offering a refractive index difference between the waveguide core and the molecule matrix. The idea was disregarded because it did not show any improvements. [26, 27]

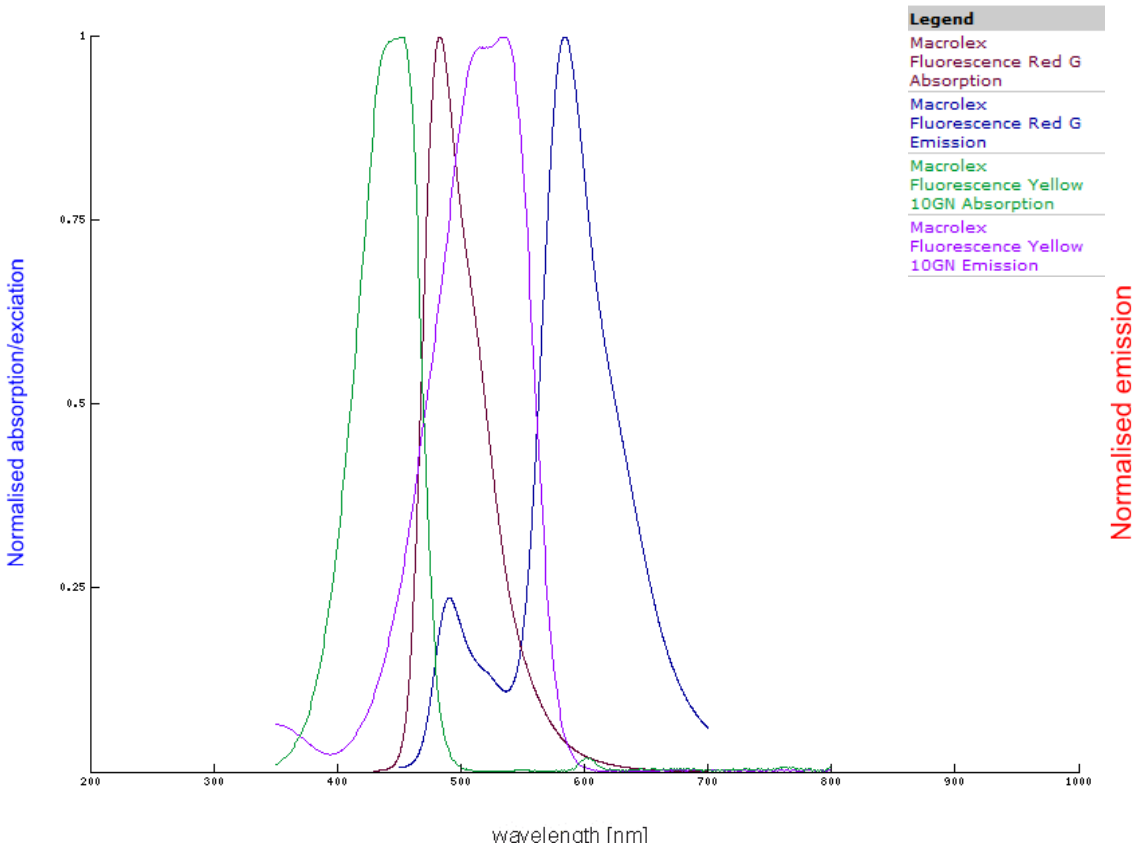

Figure 4.3: Emission and absorption spectra of Macrolex Yellow 10GN (donor) and Macrolex Red G (acceptor), both solved in chloroform. The emission spectrum of the donor and the absorption spectrum of the acceptor overlap each other. [28]

4.1.4 Titanium oxide (scattering layer)

As a scattering material titanium oxide (TiO_2), which was embedded in a polymer matrix from the Institute of Analytical Chemistry and Food Chemistry of the Graz University of Technology was used.

4.1.5 Macrolex Yellow 10GN and Macrolex Red G

The two fluorescent dyes Macrolex Yellow 10GN and Macrolex Red G form a resonance energy transfer (RET) system. Macrolex Yellow 10GN acts as the donor, Macrolex Red G as the acceptor. The emission spectrum of Macrolex Yellow 10GN overlaps the absorption spectrum of Macrolex Red G as it can be seen in Fig. 4.3. The optimization of

the RET of the two involved dyes in terms of the concentration inside a matrix material will be discussed in Sec. 4.3.1. [28]

4.2 Methods

The order of the following chapters is based on the fabrication process of the waveguiding system, giving a detailed account on the methods used.

4.2.1 Knife coating

For depositing the PDMS layer on the substrate a knife coating technique was used. The substrate was cut into pieces of the size of 20x10 cm and fixed with adhesive-tape on a glass plate. Directly after the vaccum treatment PDMS was coated onto the substrate. For that a 100 μm spiral coating knife was used to coat the substrate. After this procedure the substrate with the coated PDMS layer was baked on a hot plate for 1 hour at a temperature of 100°C to reach its final crosslinking. To allow further processing including spin-coating the PDMS-coated foil was afterwards cut into pieces of approximately 40x30 mm. Then a double-faced adhesive tape was fixed at the edges of a glass substrate with the same size and the PDMS-coated foil stuck on top of it to allow easy removal later on.

4.2.2 Plasma treatment

As mentioned before, PDMS shows a low adhesion to other materials. For this reason a 60 second O_2 plasma treatment was done with a Plasma Lab 80 Plus from the company Oxford Instruments at a power of 100 W and a pressure of 100 mTorr.

4.2.3 Spin coating

After the plasma treatment the substrates were spin coated with a 30% polystyrene in anisole mixture. A WS-650S-6NPP/Lite spin coater from Laurell Technologies Corporation was used that enables a variation of the rotation speed from 1000 to 4000 rotations per minute leading to different core thicknesses.

4.2.4 Drop coating

For the placement of the fluorescent molecules two different strategies were applied. In both of them the tip of a micropipette was dipped into the secondary emitter cocktails containing the fluorescent molecules. The droplet, which formed at the tip of the pipette, was brought into contact with the still liquid polystyrene layer directly after spin coating. Afterwards the system was cured at a temperature of 70°C for around 2 hours to evaporize to the solvent. For the other method the polystyrene layer was first cured and then the droplet was applied. This technique led to drop (named "spot" later on) diameters of about 3-5 mm.

4.2.5 Light emitting diode

As an excitation source an LED with an excitation peak of aroud 455 nm was used. Its spectrum will be shown in the following chapters.

4.2.6 Integrating sphere

After illumination of the fluorescent molecules the waveguided light is collected with an integrating sphere ISP250-110 and then spectrally analyzed by a CAS 140 CT Compact Array Spectrometer (both instruments from Instrument Systems).

4.2.7 Resonance energy transfer measurement

To be able to optimize the resonance energy transfer secondary emitters, solutions with different concentrations of Macrolex Yellow 10GN and Macrolex Red G in the matrix material ethylcellulose were prepared as described in Sec. 4.3.1. As a solvent a mixture of toluene/ethanole in the ratio of 8:2 was used and the ratio solid materials (ethylcellulose, Macrolex) to liquid materials (toluene/ethanol) was held constant to achieve comparable thicknesses when spin-coating the solutions on a glass substrate. The coated slides were then analyzed with a Shimadzu RF-5301 PC spectrofluorophotometer with and illumination wavelength of 450 nm.

4.2.8 Optical microscope

Microscopic images were taken with an Olympus BX51 Microscope, which was also used to specify the thicknesses of the substrate/PDMS/Polystyrene-stack. The fluorescent molecules were excited by an LED and an image of the cross-section of the waveguide system was taken showing the illuminated core material. The calibrated microscope allowed distance measurements on the image.

4.3 Experimental data and analysis

This section describes and interprets the experimental results. Besides the optimization of the resonance energy transfer (RET), a thickness variation of the core material was done, two different drop coating techniques were compared, the intensity of the excitation source was varied and an out-coupling technique was studied using TiO_2 scattering layers.

4.3.1 Macrolex resonance energy transfer optimization

When using fluorescent molecules to couple light into a waveguide the optimization of the involved RET-system is important. Besides the spectral overlap and the orientation of the molecules, their mutual distance and the concentration of the donor and the acceptor in the matrix material play an important role. By a varation of the concentration the energy transfer can be optimized for the usage as a secondary emitter. As described in Sec. 4.2.7 different solutions containing Macrolex Yellow 10GN and Macrolex Red G in ethylcellulose were prepared. First, four different Macrolex Yellow 10GN concentrations ranging from 1% to 4% were set up. The important parameters can be seen in Tab. 4.1. The spectra (measured with a spectrofluorophotometer) of the four spin coated glass slides are presented in the upper picture of Fig. 4.4. In can be clearly seen that the cocktail containing 2% Macrolex Yellow 10GN shows the highest fluorescence intensity. Note that the maximum of the emission lies at around 490 nm.

After the optimization of donor Macrolex Yellow the value of 2% was held constant and now the concentration of the acceptor molecule Macrolex Red G was varied. Three different concentrations were prepared, 0.3%, 0.5% and 0.7% in ethylcellulose. In the lower graph of Fig. 4.4 can be seen that the solution with 0.3% Macrolex Red G and 2% Macrolex Yellow 10GN clearly shows the highest fluorescence signal. Furthermore, the maximum of the emission spectrum has shifted from 490 nm to around 580 nm (Stokes shift). The emission of the donor molecule has nearly disappeared due to the energy transfer in the system. The amount of Macrolex Yellow 10GN is expected to be low

Table 4.1: Parameters for the optimization of the concentration of Macrolex Yellow 10GN in ethylcellulose. The total mass of solids ($m_{sol} = m_{EC} + m_{MLY}$) in toluene ($m_{tol}$) was kept constant, while the masses of Macrolex Yellow 10GN (m_{MLY}) and ethylcellulose (m_{EC}) were varied. This led to a concentration (MLY[EC]) of 1%-4% Macrlex Yellow 10GN in ethylcellulose.

m_{MLY}[g]	m_{EC}[g]	m_{sol}[g]	m_{Tol}[g]	MLY[EC]	solid/liquid
0.0005	0.0495	0.05	5	1%	1/100
0.001	0.049	0.05	5	2%	1/100
0.0015	0.0485	0.05	5	3%	1/100
0.002	0.048	0.05	5	4%	1/100

Table 4.2: Parameters for the optimization of the concentration of Macrolex Red G in ethylcellulose. The total mass of solids ($m_{sol} = m_{EC} + m_{MLY} + m_{MLR}$) in toluene ($m_{tol}$) was kept constant, while the masses of Macrolex Red G (m_{MLR}) and ethylcellulose (m_{EC}) were varied at a constant mass of Macrolex Yellow 10GN (m_{MLY}). This led to a concentration (MLR[EC]) of 0.3%-0.7% Macrolex Red G and a constant concentration (MLY[EC]) of 2% Macrolex Yellow 10GN in ethylcellulose.

m_{MLR}[g]	m_{MLY}[g]	m_{EC}[g]	m_{sol}[g]	m_{Tol}[g]	MLR[EC]	MLY[EC]
0.00015	0.001	0.04885	0.05	5	0.3%	2%
0.00025	0.001	0.04875	0.05	5	0.5%	2%
0.00035	0.001	0.0465	0.05	5	0.7%	2%

enough to minimize self absorption, while on the other hand the molecules Macrolex Yellow 10GN and Macrolex Red G should be in close proximity to allow the resonance energy transfer.

4.3.2 Description of the waveguiding system

The fabrication technique for the waveguiding system was discussed above. Figure 4.5 summarizes the two basic sample arrangements. On top of the substrate including the absorbing material the two layers were (PDMS and Polystyrene) deposited. The secondary emitter fluorescent molecules couple modes into the waveguide after being excited by an LED. The molecules were deposited by the drop coating technique introduced in Sec. 4.2.4. Two different out-coupling mechanisms (see Fig. 4.5) are shown including edge coupling and out-coupling by TiO_2. For all measurements an integrating sphere was used. The edge of each sample was put into the sphere for a few millimeters, an aperture was closed to avoid stray light, and the light emerging from the edge of the

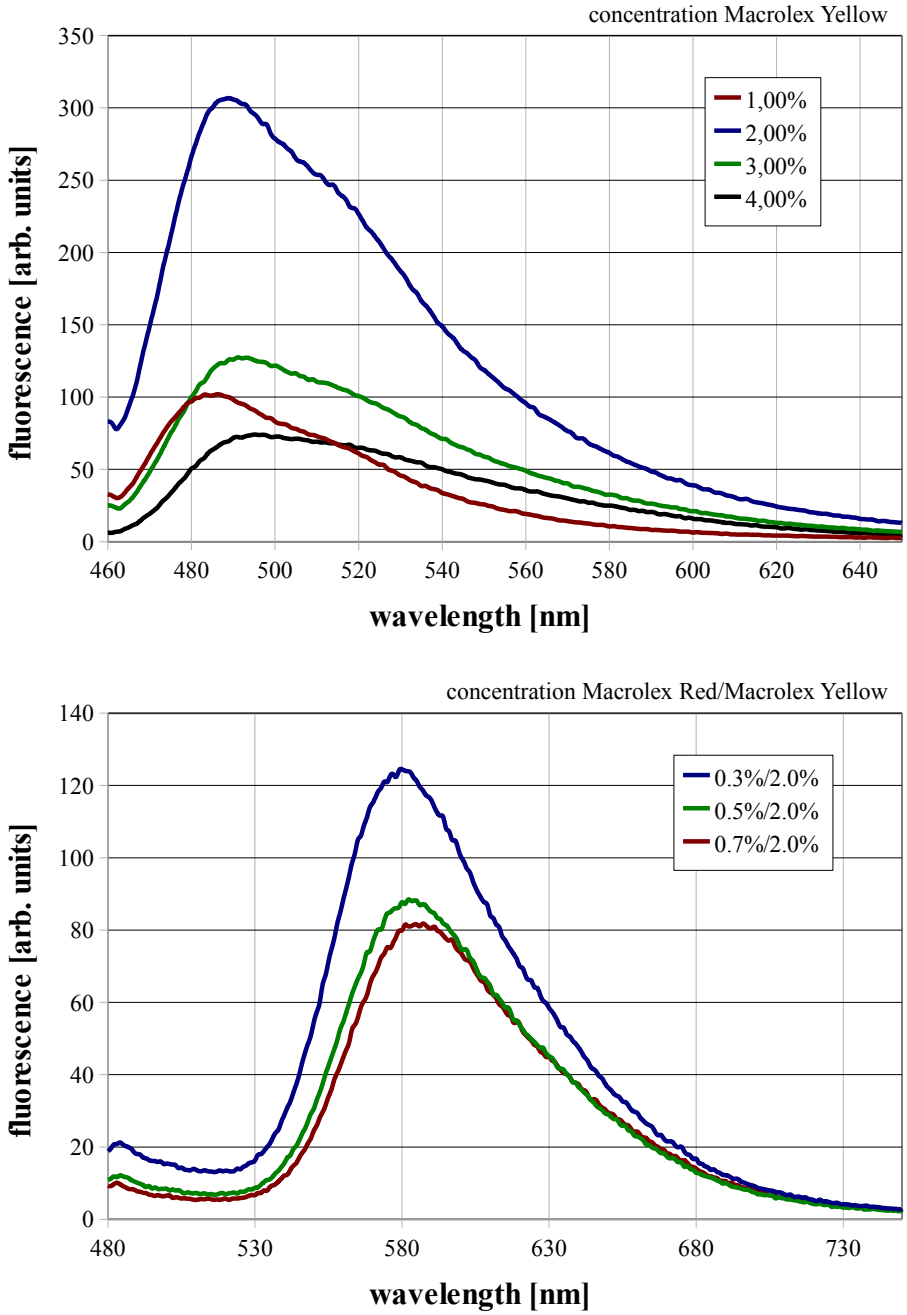

Figure 4.4: Fluorescence spectra in dependence of the concentration of Macrolex Yellow 10GN [%] in ethylcellulose (upper panel). Fluorescence spectra in dependence of the concentration of Macrolex Red G [%] / Macrolex Yellow 10GN [%] in ethylcellulose (lower panel).

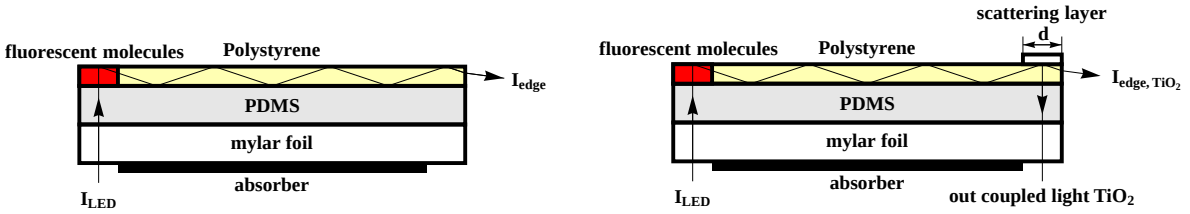

Figure 4.5: Comparison of two different out-coupling methods. LED light is coupled into the waveguide via fluorescent molecules and coupled out at the edge of the waveguide I_{edge} (left hand side). On the right hand side a part of the light is coupled out by TiO_2 placed on top of the waveguide, while some amount of the light leaves the waveguide at the edge (I_{edge,TiO_2}).

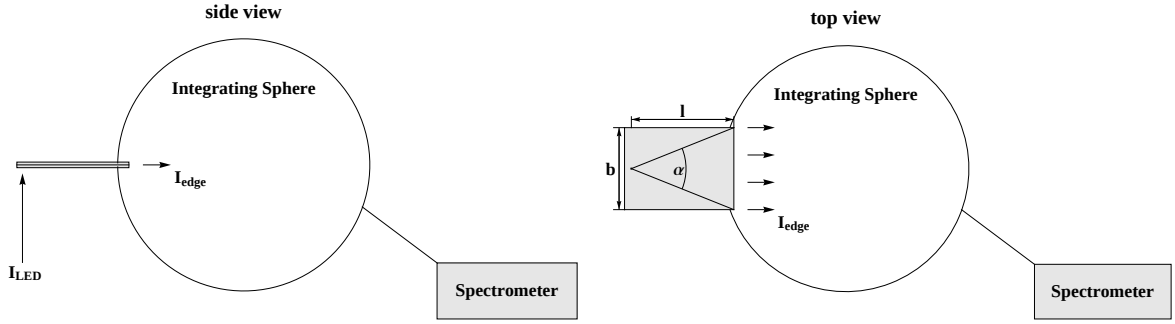

Figure 4.6: Side view and top view of the setup for measuring the intensity emitted from the edge of the waveguide I_{edge}. The fluorescent molecules are excited by an LED. The out-coupled light is collected by an integrating sphere and analyzed by a spectrometer. Only the molecules emission within an angle α radiates into the integrating sphere.

waveguide was measured by the integrating sphere with an integration time of 65 seconds. The excitation spectra were also determined but at a lower integration time of 65 ms. The according intensities (I_{LED} and I_{edge}) were evaluated by integrating the spectra over the wavelength. A side and a top view of the measurement setup can be seen in Fig. 4.6. To be able to compare samples of different size the throughput was calculated according to Eq. (4.1). As only an angle α radiates into the integrating sphere, the measurement of the width b and the distance l of the system is needed to calculate the throughput for a full 360°.

$$TP\,[\%] = 100\frac{\pi}{\arctan\frac{b}{2l}}\frac{I_{Edge}}{I_{LED}} \tag{4.1}$$

4.3.3 Position of the fluorescent molecules

As seen in Sec. 2.2.3, the position of the molecules influences the irradiation characteristics. In particular, the distance of the molecules to the center of the waveguide is expected to influence the amount of light which is coupled in. This should be given geometrically due to the fact that the acceptance angle gets smaller if the secondary emitter is far away from the waveguide axis and less light is radiated beyond the critical angle. Two different drop coating fabrication methods were studied as mentioned in Sec. 4.2.4 to find out if it is favourable to include the molecules inside the core material or not. Dropping the fluorescent dyes in the still liquid polystyrene layer direcectly after spin coating is named "spot inside core" and placing them on the cured polystyrene layer is called "spot on top of core". For both measurements the size (l=35 mm, b=30 mm) and thickness (h=17 μm) of the waveguide was held constant. Figure 4.7 clearly points out that at a constant waveguide configuration with the same exitation LED-intensity (lower panel of Fig. 4.7) molecules inside the core material have to be favoured. Integrating over the curves and using Eq. (4.1) yields a throughput of around 3.4%, if the molecules are inside the core material, compared to 1.1% with the molecules on top of the polystyrene layer. A microscope image of a 17 μm waveguide is shown in Fig. 4.8 for two different exposure times. The substrate, cladding and core materials can be easily identified.

4.3.4 Thickness variation of the polystyrene core

To demonstrate the influence of the number of propagating modes on the throughput, a variation study of the thickness of the core material was done. Section 4.3.3 suggests using a spot located inside the core material, which was done in all of the following experiments. Three different rotational speeds (2000 rpm, 3000 rpm, 4000 rpm) were used to coat polystyrene on the PDMS layer, leading to thicknesses between 10 μm and 17 μm. The thickness measurement was done with a calibrated light microscope as mentioned in Sec. 4.2 while illuminating the secondary emitter spot. Table 4.3 shows the parameters of the three investigated thicknesses, in Fig. 4.9 the three spectra are presented. At 17 μm the throughput reaches a maximum of 2.6%. From Eq. (2.53) the number of modes in the waveguide can be estimated at a wavelength of 650 nm, as included in Tab. 4.3. The solution is equal to the number of modes calculated in Sec. 3.1 by analyzing the transcendental equation.

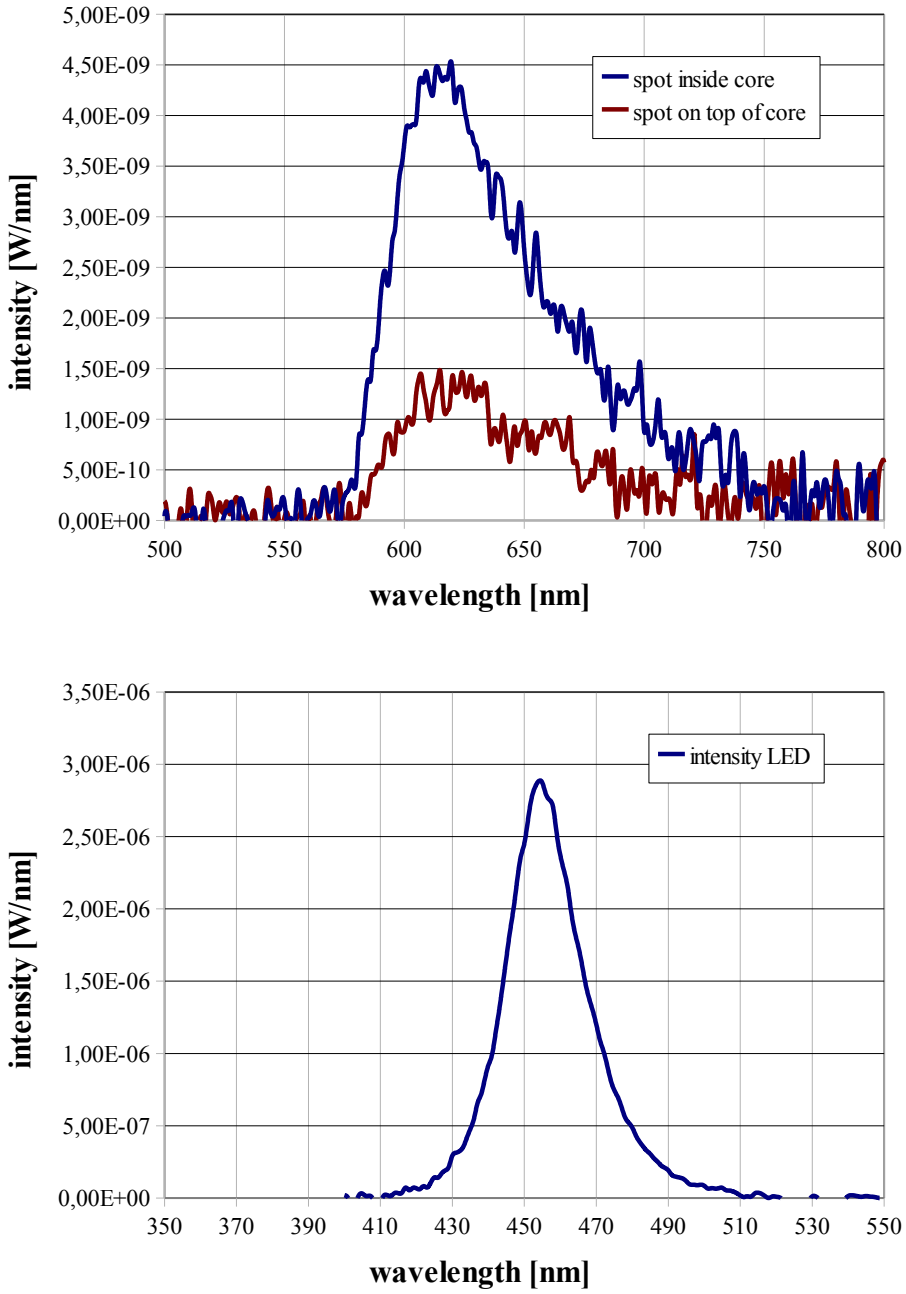

Figure 4.7: Influence of the spot postion on the fluorescence spectra. Two drop coating techniques were compared, either putting the fluorescent molecules on the cured polystyrene layer (spot on top of core) or droping them in the liquid polystyrene layer directly after spin coating (spot inside core). The lower picture shows the spectrum of the LED excitation source.

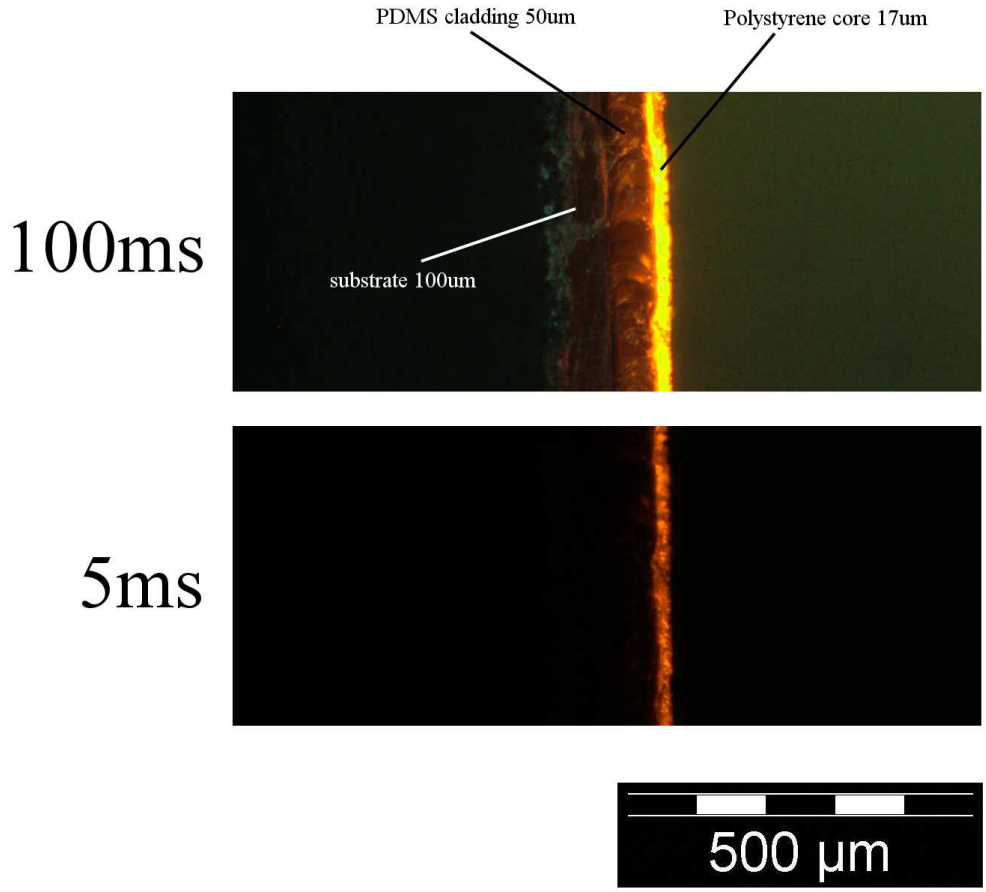

Figure 4.8: Microscope images of the cross-section of the waveguide system taken with two exposure times. For 100ms exposure time the three layers polystyrene/PDMS/substrate can be clearly seen. At an exposure time of 5 ms just the polystyrene waveguide is visible.

Table 4.3: Influence of the thickness of the polystyrene core on the throughput together with the estimated number of modes according to Eq. (2.53).

rpm	thickness h	length l	width b	throughput TP	modes M
2000	17 μm	35 mm	30 mm	2.6%	37
3000		35 mm	30 mm	1.9%	
4000	10 μm	31 mm	30 mm	1.0%	22

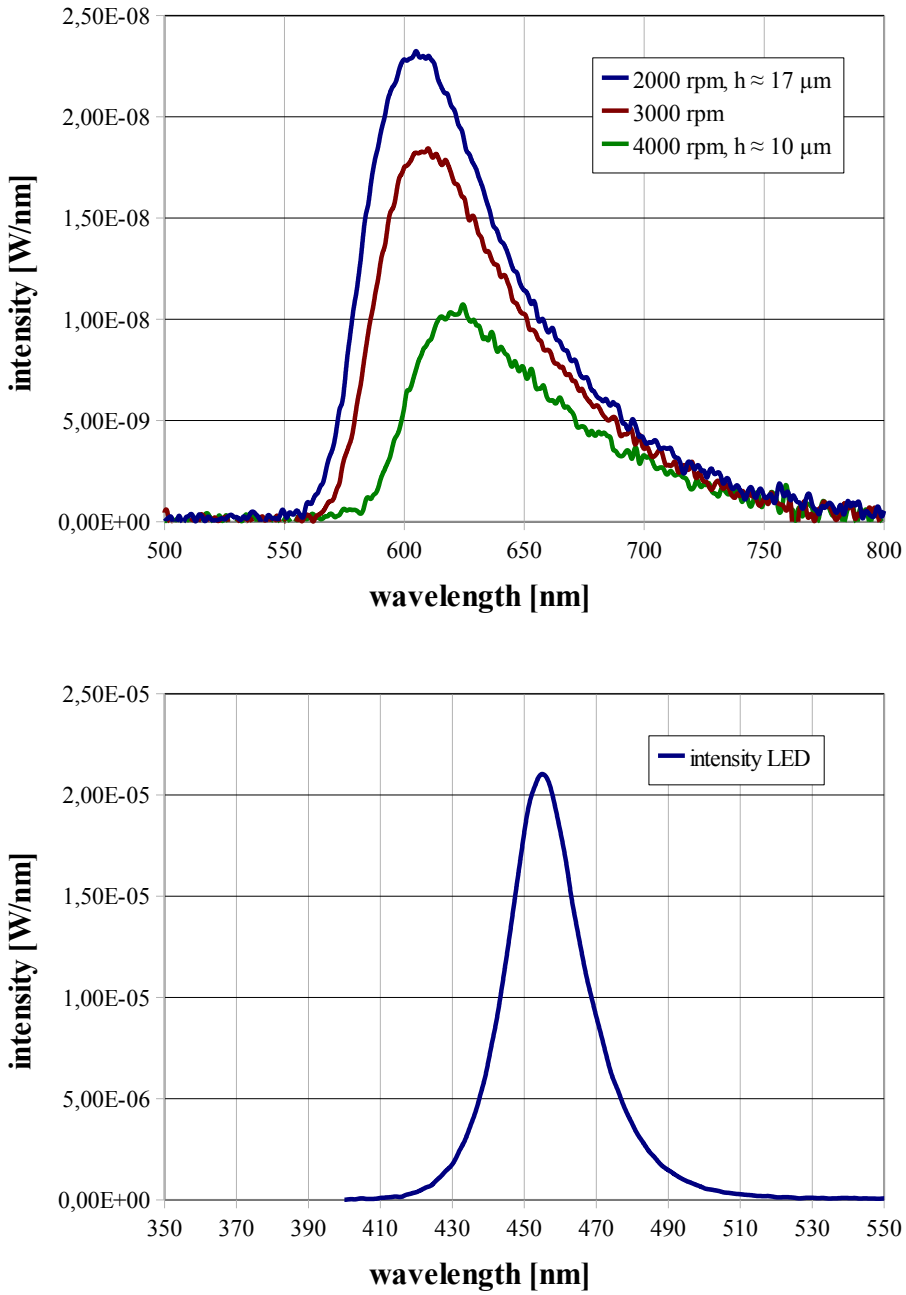

Figure 4.9: Fluorescence spectra in dependence of the thickness of the core material. Three different rotation speeds of the spin coater were compared leading to thicknesses between 10 μm and 17 μm. The lower panel shows the spectrum of the LED excitation source.

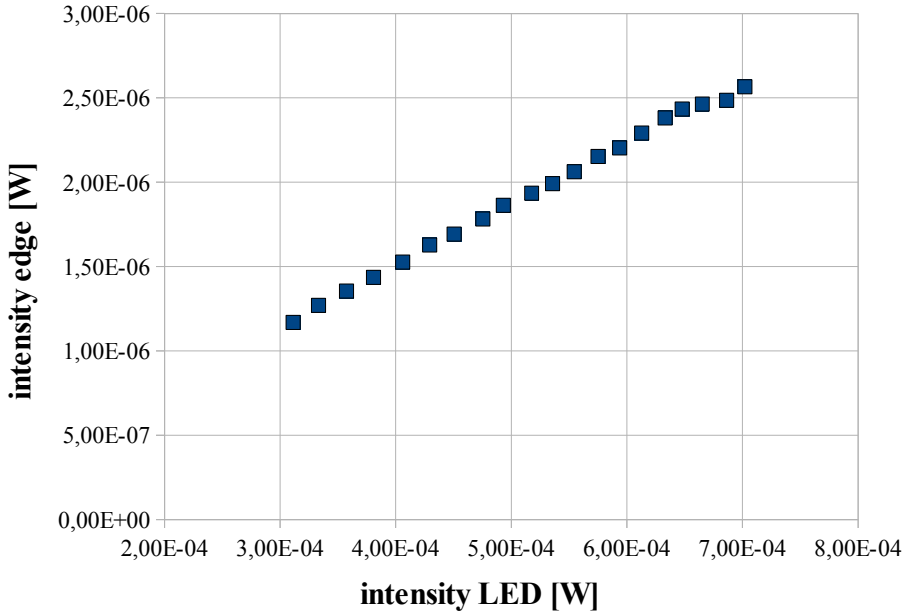

Figure 4.10: Edge intensity in dependence of the excitation intensity for a 17 μm waveguide. The throughput stays constant as the ratio I_{edge}/I_{LED} is constant.

4.3.5 Intensity variation of the light emitting diode

To find out if the intensity of the LED excitation source has any influence on the light throughput, a standard sample (polystyrene on PDMS, 17 μm, l=36 mm, b=30 mm) was examined. The signal I_{edge} was measured while the current of the LED was raised from 250 mA to 725 mA in steps of 25 mA, while the voltage was held constant. Afterwards the spectrum for each LED current was measured to determine the LED intensity I_{LED} at each current. From Fig. 4.10 it can be seen that the ratio I_{edge}/I_{LED} remains constant and therefore the throughput also remains the same. It is important to note that the intensity I_{edge} refers - as usual - to the amount of light emitted to a certain acceptance angle (compare Fig. 4.6).

4.3.6 Attenuation due to titanium oxide layers

For the integration in the optical waveguide sensor platform discussed in the introduction a 90° deflection to the organic photodiode is necessary. An out-coupling method using TiO_2 on top of the core material is investigated in this chapter. At the right end of the waveguide (compare Fig. 4.5) a TiO_2 scattering layer with a length d is painted on the waveguide. A part of the light now is coupled out by the scattering layer and

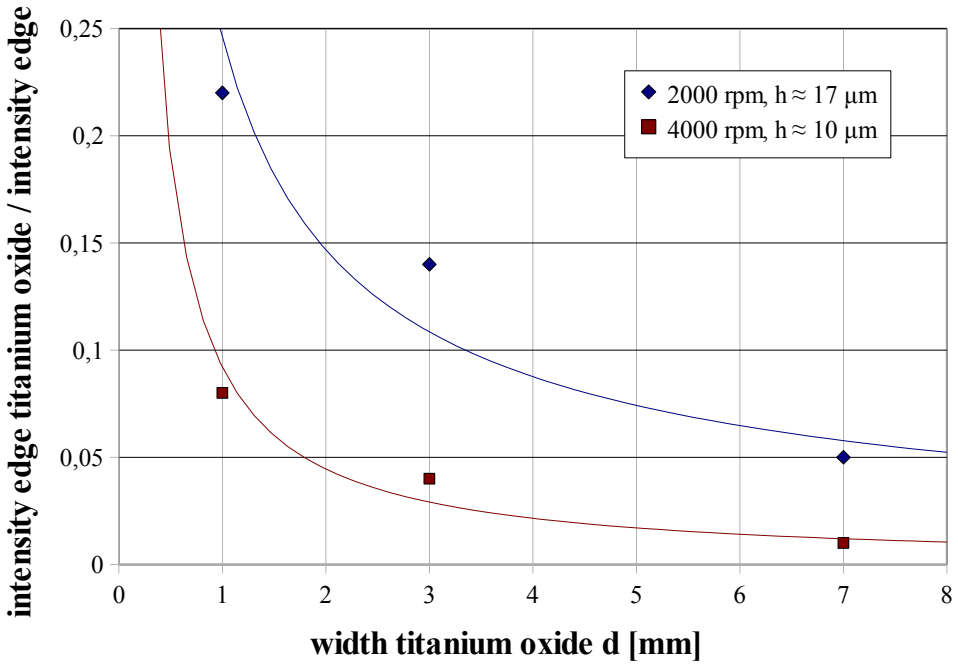

Figure 4.11: Titanium oxide induced attenuation of the edge intensity for two different core thicknesses of 10 μm and 17 μm. At a scattering length of 1 mm the signal emerging from the edge of the waveguide is attenuated by 78%. The lines are guides to the eye.

deflected downwards (out-coupled light TiO_2) while some amount is still leaving the edge (I_{edge,TiO_2}). This amount is now measured with the integrating sphere and compared to the signal without scattering particles ($I_{edge}/I_{edge,TiO_2}$). For both measurements (with and without TiO_2) the position of the waveguide in relation to the integrating sphere is identical. From the attenuation of the signal it can be inferred which amount of light is coupled out by the scattering molecules. The measurement was done for three different scattering layer lengths (1 mm, 3 mm, 7 mm) and two core thicknesses (10 μm and 17 μm).

It can be clearly seen that even at a scattering layer length of d=1 mm using a waveguide thickness of 17 μm the signal leaving the edge of the waveguide is attenuated by around 78%. For longer scattering lengths the signal is reduced to a few percent, indicating that almost everything is coupled out by the scattering layer. Using a thinner waveguide of 10 μm makes the out-coupling even more efficient. A scattering length of 1 mm attenuates the edge-signal for example by around 92%.

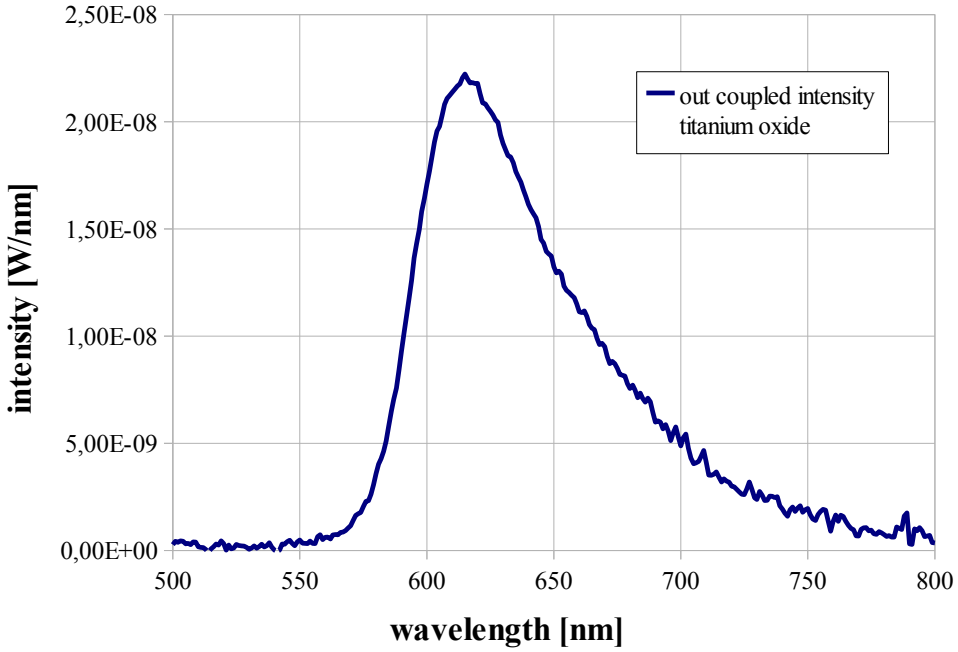

Figure 4.12: Spectrum of a 1 mm TiO_2 layer placed on top of a 17 μm waveguide. Proof of principle that out-coupling by a scattering layer can be directly measured.

4.3.7 Verification of out-coupling via titanium oxide

As a proof of principle for the out-coupling ability of the TiO_2 layer its spectrum is shown (comapare "out coupled light TiO_2" in Fig. 4.5). For a 17 μm waveguide with l=35 mm and b=30 mm, at l_1=20 mm, a 1 mm TiO_2 layer was painted on the core and the spectrum of the scattered light measured with the integrating sphere (see Fig. 4.12). By using Eq. (4.1) we find a throughput of around 3%. This measurement was not very exact, because the sample was turned by 90° and the aperture of the intergrating sphere had to be opened to allow the light from the scattering particles to enter the sphere. On the other hand the aperture should be closed as far as possible to avoid stray light. Anyhow it shows that the light from scattering particles can be detected directly by the integrating sphere.

4.3.8 Explanatory notes on the fabrication process

The presented drop coating technique has the problem that the amount of secondary emitters placed on the waveguide layer will hardly be constant as everything is done by hand and the droplet had to be brought in contact to the surface. The large viscosity of

the secondary emitter solution did not allow the usage of high-prescition pipettes. The amount of light which is coupled into the waveguide is expected to be strongly dependent on the size and homogenity of the fluorescent molecule spot.

Another issue is the adhesion of polystyrene on PDMS. The plasma treatment routine chosen does not offer ideal adhesion. In fact, for most of the waveguides, the polystyrene layer started to peel off the PDMS after a few days. For coupling measurements this durability is sufficient. An optimization of the plasma parameters is a topic to be further investigated.

Furthermore, an element of uncertainty is the way the waveguide was cut. Cutting is necessary to remove elevations which form at the outer parts of the waveguide during spin coating. A simple pair of scissors was used, but the cross-section is not expected to be homogenous and the out-coupling may vary.

Chapter 5

Summary and Outlook

As an introduction to the simulation and experimental section a comparison of geometrical with electromagnetic waveguiding theory was presented. Two different derivations, one of them using the wave equation together with the Maxwell equation boundary conditions, the other one using interference, led to the transcendental equation and the concept of optical modes. Coupling mechanism to waveguides, with a special focus on fluorescent molecules, were presented.

With the ray tracing simulation software ZEMAX the propagation of light originating from a point source inside a planar waveguide was investigated. The throughput of a waveguide was simulated for different propagation conditions. For a core/cladding system comparable to the one used in the experimental section (refractive indices of 1.59 and 1.42) the throughput approaches a constant value of around 47%. In a symmetric waveguide without cladding surrounded by air the throughput reaches 78%. When comparing the intensity of the signal inside and outside of the waveguide it stands out that after a certain propagation length more than 90% of the signal is coupled out. Nevertheless 100% is not reached, due to Fresnel reflection. By evaluating the transcendental equation with Mathematica the basic shape of modes inside such a waveguide was derived.

A novel planar waveguide system was used to demonstrate in-coupling of light by using fluorescent molecules and out-coupling by scattering molecules. First, the resonance energy transfer system Macrolex Yellow/Macrolex Red was optimized by finding the optimal concentration inside the matrix material ethylcellulose. A value of 2% Macrolex Yellow and 0.3% Macrolex Red gives the highest fluorescence signal together with a Stokes shift of around 130 nm relative to the absorption wavelength of 450 nm. Comparing two investigated drop coating techniques it turns out that it is favourable to deposit the fluorescent molecules inside the core material directly after spin coating when the core layer is still liquid. The thickness of the core material directly influences the throughput, a thicker waveguide leads to a higher throughput. The throughput in a 17 μm waveguide is about 2.5 times larger than in a 10 μm waveguide. Varying the

intensity the excitation source, a light emitting diode, turns out not to influence the throughput. Scattering layers couple out almost all of the light. Even for a scattering length of only 1 mm at a waveguide thickness of 17 μm the signal emerging from the edge of the waveguide is reduced by around 78%. A thinner waveguide couples out light more efficient.

For the pratical usage in sensing technology the integrated waveguide should undergo several improvements. The drop coating technique could be replaced by inkjet printing to allow precise arrangements of an exact amount of fluorescent molecules. Furthermore, a variation of the matrix material in which the secondary emitters are embedded would be interesting. Roll-to-roll processing could offer a fast production technique. The measurements with the integrating sphere might be compared to a method using a modulated signal together with a lock-in amplifier to suppress stray light. As an alternative to fluorescent molecules, prisms or gratings which are stamped onto the waveguide structure could be interesting. All these techniques promise interesting developments in the future of integrated optical waveguide sensing.

List of Figures

List of Tables

Bibliography

[1] Torsten Mayr, Tobias Abel, Barbara Enko, Sergey Borisov, Christian Konrad, Stefan Köstler, Bernhard Lamprecht, Stefan Sax, Emil J. W. List, and Ingo Klimant. A planar waveguide optical sensor employing simple light coupling. *Analyst*, 134:1544–1547, 2009.

[2] ISOTEC. Integrated Organic Sensor and Optoelectronic Technologies. `http://www.isotec-cluster.at/`, accessed on 2010/06/01.

[3] Wolfgang Bludau. *Lichtwellenleiter in Sensorik und optischer Nachrichtentechnik*. Springer-Verlag Berlin Heidelberg New York, 1998.

[4] Encyclopedia Britannica. Fermats principle. `http://www.britannica.com/EBchecked/topic/204700/Fermats-principle`, accessed on 2010/05/22.

[5] Dieter Meschede. *Optik, Licht und Laser*. B. G. Teubner, 1999.

[6] Bahaa E. A. Saleh and Malvin Carl Teich. *Grundlagen der Photonik*. WILEY-VCH Verlag, Weinheim, 2nd edition, 2008.

[7] Lukas Novotny and Bert Hecht. *Principles of Nano-Optics*. Cambridge University Press, 2nd edition, 2006.

[8] NSG Europe. Selfoc lenses. `http://www.nsgeurope.com/products.shtml`, accessed on 2010/06/02.

[9] Eugene Hecht. *Optics*. Addison Wesley, 4th edition, 2002.

[10] Katsunari Okamoto. *Fundamentals of Optical Waveguides*. Elsevier, 2nd edition, 2006.

[11] Clifford R. Pollock and Michal Lipson. *Integrated Photonics*. Kluwer Academic Publishers, 2003.

[12] Safa O. Kasap. *Optoelectronic devices and photonics : principles and practices*. Prentice-Hall, Inc., 2001.

[13] Theodor Tamir. *Integrated optics. Topics in applied physics*, volume 7. Springer-Verlag Berlin Heidelberg New York, 1975.

[14] Rüdiger Paschotta. Encyclopedia of laser physics and technology - multimode fibers. `http://www.rp-photonics.com/multimode_fibers.html`, accessed on 2010/02/25.

[15] Matt Young. *Optik, Laser, Wellenleiter*. Springer-Verlag Berlin Heidelberg New York, 1997.

[16] Tobias Abel. Enhancing Sensor Performance by means of new sensor design and excitation strategies. Master's thesis, Institute of Analytical Chemistry and Radiochemistry, Graz University of Technology, 2008.

[17] Bernard Valeur. *Molecular Fluorescence - Principles and Applications*. WILEY-VCH Verlag, Weinheim, 2002.

[18] Barbara Enko. New geometries and mechanisms to enhance optical sensor performance. Master's thesis, Institute of Analytical Chemistry and Radiochemistry, Graz University of Technology, 2008.

[19] Daniel M.C Koller. *Luminescence coupling to dielectric and metallic interfaces*. PhD thesis, Institute of Physics, Karl-Franzens University Graz, 2009.

[20] Optima Reseach Ltd. Optima Research ZEMAX. `http://www.optima-research.com/Software/Optical/Zemax/overview.htm`, accessed on 2010/03/12.

[21] Stefan Stögner. Untersuchung alternativer optischer Komponenten für die Einkopplung in Lichtwellenleiter. Master's thesis, Institut für Breitbandkommunikation der Technischen Universität Graz, 2009.

[22] Jan Roth. *Funktionalisierung von Silikonoberflächen*. PhD thesis, Fakultät Mathematik und Naturwissenschaften der Technischen Universität Dresden, 2009.

[23] D. Fuard, T. Tzvetkova-Chevolleau, S. Decossas, P. Tracqui, and P. Schiavone. Optimization of poly-di-methyl-siloxane (pdms) substrates for studying cellular adhesion and motility. *Microelectronic Engineering*, 85:1289–1293, 2008.

[24] Sonja Pichler. *Funktionelle Materialien zur Herstellung optischer Wellenleiter*. PhD thesis, Technische Universität Graz, 2007.

[25] Suter swiss-composite group. `http://www.swiss-composite.ch/`, accessed on 2010/02/19.

[26] James E. Mark. *Polymer Data Handbook*. Oxford University Press, Inc., 1999.

[27] Hong Ma, Alex K. Y. Jen, and Larry R. Dalton. Polymer-based optical waveguides: Materials, processing, and devices. *Advanced Materials*, 14(19):1339–1365, October 2002.

[28] Fluorophores.org - the database of fluorescent dyes and applications. `http://www.fluorophores.tugraz.at/`, accessed on 2010/03/20.